Received: 24 April 2020 | Revised: 22 July 2020 | Accepted: 1 August 2020

DOI: 10.1111/ffe.13327

INVITED CONTRIBUTION

FFEMS Fatigue & Fracture of Engineering Materials & Structures WILEY

Fracture toughness of rigid polymeric foams: A review

Liviu Marşavina | **Emanoil Linul**

Department of Mechanics and Strength of Materials, University Politehnica Timisoara, Blvd. Mihai Viteazu, No.1, Timisoara, 300 222, Romania

Correspondence
Liviu Marşavina, Department of Mechanics and Strength of Materials, University Politehnica Timisoara, Blvd. Mihai Viteazu, No.1, Timisoara 300 222, Romania.
Email: liviu.marsavina@upt.ro

Funding information
European Commission, Grant/Award Number: Horizon 2020, No. 857124; Romanian Ministry of Research and Innovation, Grant/Award Numbers: 10PFE/16.10.2018, PERFORM-TECH-UPT, PN-III-P1-1.2-PCCDI-2017-0391

Abstract

Polymeric foams have good capacity of absorbing energy in compression but are brittle in tension. Linear elastic fracture mechanics is successfully applied to assess the integrity of polymeric foam-based composite structures. The fracture toughness represents an important parameter. The different approaches to estimate the fracture toughness of polymeric foams are reviewed: analytical and numerical micromechanical models and experimental investigations. Focus is given on the parameters influencing the fracture toughness of polymeric foams like specimen type, solid material, density, loading speed, size effect and temperature. Data on mixed-mode loading and dynamic fracture toughness are also presented. The last part of the paper presents some results to increase the fracture toughness by reinforcing of polymeric foams.

KEYWORDS

experimental data, fracture toughness, micromechanical models, mixed-mode fracture, numerical analysis, polymeric foams

1 | INTRODUCTION

The polymeric foams belong to the class of manufactured cellular materials (Figure 1). The properties of cellular materials depend on the properties of the solid from which they are produced; the cell shapes, dimensions and topology and the relative density (density of the foam divided to density of solid material) (Figure 2).[1]

Polymeric foams are made of interconnected networks of solid struts and cell walls incorporating voids with entrapped gas, resulting a cellular structure with open (the solid material is found in the edges of the cells), closed (the solid material is found in both the edges and faces of the cells) or mixed (partially open, partially closed) cells. The main characteristics of foams are lightweight, high porosity, good energy absorption capacity and floatability.[2,3] The use of polymeric foams increases considerably in the last three decades. The main applications are in construction and civil engineering for thermal isolation, in packing, in aeronautics and automotive industries, in buoyancy due to their floatability and in sport for shoes, helmets and other protection systems.

Most of the plastic foam materials crush progressively in compression until they reach full densification,[2] whereas in tension fail by propagating of a single crack.[4] Polymeric foams have an elastic–plastic behaviour in tension, whereas in the presence of notches and cracks, they behave linear-elastic up to fracture and highlight a brittle failure.[4,5] Therefore, they can be treated using linear elastic fracture mechanics (LEFM) criteria. Consequently, the fracture toughness of such porous materials became an important characteristic, because cracks weaken the foam structures capacity of carrying load.

The objective of this paper is to review the analytical, numerical and experimental studies carried on to determine the fracture toughness of rigid polymeric foams.

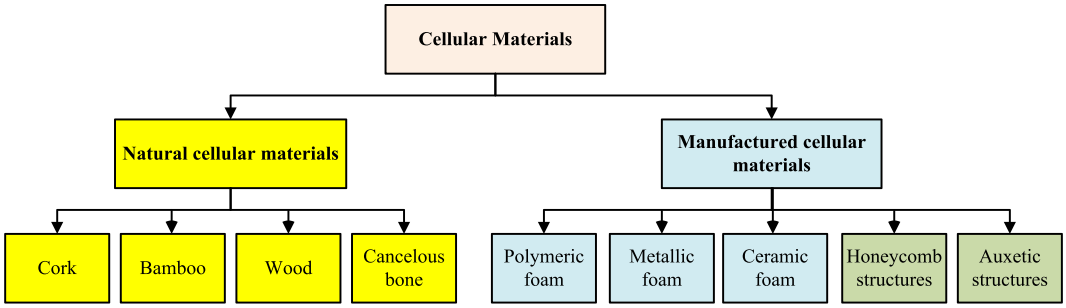

FIGURE 1 Classes of cellular materials, adapted from Ashby[1] and Gibson and Ashby[2] [Colour figure can be viewed at wileyonlinelibrary.com]

Particular attention will be paid to the effects of density, anisotropy, loading speed, specimen type and temperature on fracture toughness. The mixed-mode fracture, the size effect on polymeric foam and dynamic loading will be also presented. Finally, some new methods of increasing the fracture toughness by reinforcing the foams are discussed.

2 | MICROMECHANICAL MODELS FOR FRACTURE TOUGHNESS OF FOAMS PREDICTION

Micromechanical models are often used to predict the properties of cellular materials,[2] such as foams Pr_f, based on the properties of solid material Pr_s and the relative density ρ_f/ρ_s:

$$\mathrm{Pr}_f = C\mathrm{Pr}_s\left(\frac{\rho_f}{\rho_s}\right)^n \tag{1}$$

where C and n are fitting parameters.

Micromechanical analysis can estimate the full multiaxial properties and response of cellular materials, which are usually anisotropic.[6–12] Such properties are often difficult to measure experimentally, but they are very important in design of the lightweight composite structures containing foam cores. Micromechanical analysis also allows to describe the structural damage and failure of cellular materials.[13–21] Gibson and Ashby,[2] Mills[3] and Fleck et al.[22] presented extensive studies of micromechanical models for cellular materials. In this chapter, only the main models regarding the fracture toughness will be reviewed.

The micromechanical models used to predict the fracture toughness K_{IC} of the foams are based on the fracture strength of the cell wall materials σ_{fs}, the relative density ρ_f/ρ_s and the cell dimension l.[23] Gibson and Ashby[2] assumed that the crack tip is located at half-edge and advances discrete with one cell width (Figure 3). Applying a tensile load to cellular structure, the cell walls deform elastically in mode I, and load is transmitted through the foam as a set of forces and moments acting on the cell edges.

Considering that the crack extends when the tensile strength on the strut reaches the fracture strength of the solid material, Maiti et al.[24] proposed the following micromechanical models:

- for open cells

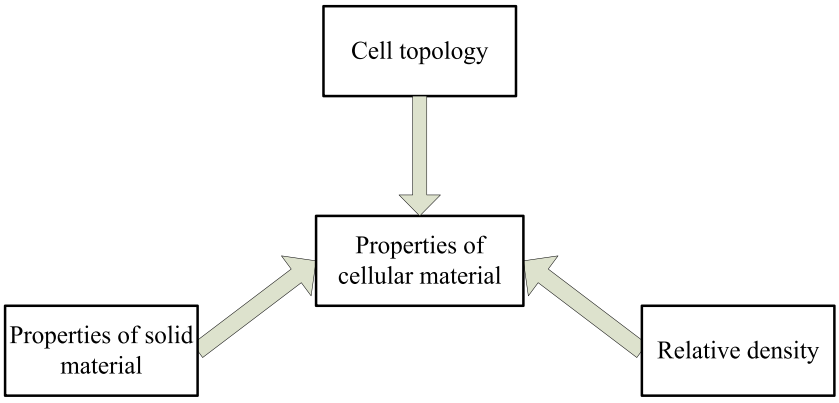

FIGURE 2 Factors influencing the cellular material properties, adapted from Ashby[1] [Colour figure can be viewed at wileyonlinelibrary.com]

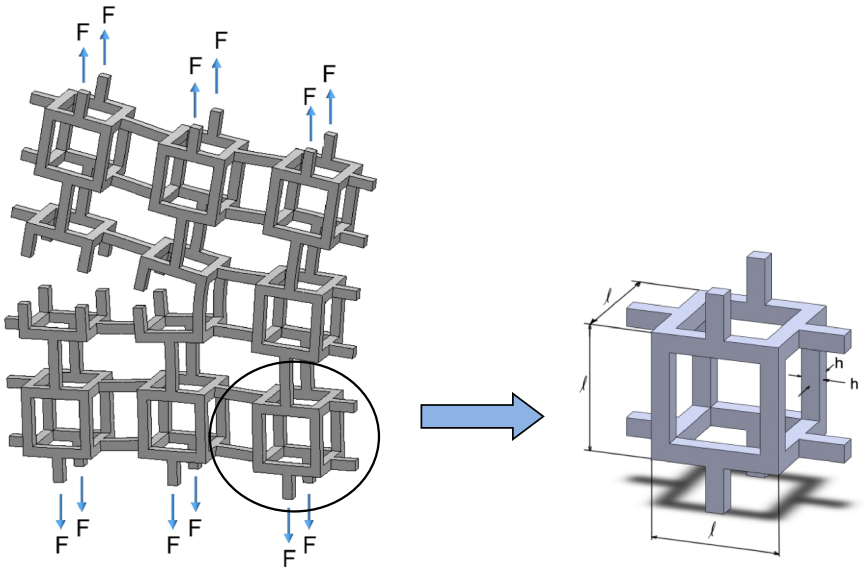

(A) crack propagation trough brittle open-cell foam[2] (B) unit cell

FIGURE 3 Cracked cellular structure, adapted from Gibson and Ashby[2] [Colour figure can be viewed at wileyonlinelibrary.com]

$$K_{IC} = C_1 \sigma_{fs} \sqrt{\pi l} \left(\frac{\rho_f}{\rho_s}\right)^{1.5} \tag{2a}$$

- for closed cells

$$K_{IC} = C_2 \sigma_{fs} \sqrt{\pi l} \left(\frac{\rho_f}{\rho_s}\right)^{2} \tag{2b}$$

where C_1 and C_2 are proportionality constants. For determining the constant C_1 from Equation 2a, a series of experimental data obtained for different foam materials such as polyurethane,[25,26] PMMA[24] and ceramic[27] were interpolated, resulting $C_1 = 0.65$.

Huang and Gibson[28,29] investigated the factors affecting the fracture toughness of brittle honeycombs and foams. Experimental results on reticulated carbon foams show that Equations 2a and 2b are valid only for crack length higher than 10 times the cell length.[28]

Green[30] proposed a similar correlation considering elastic deformation in shell theory of hollow sphere model for foam cells:

$$\frac{K_{IC}}{\sigma_{fs}\sqrt{\pi l}} = 0.28 \left(\frac{\rho_f}{\rho_s}\right)^{1.3} \tag{3}$$

Choi and Sankar[31] using LEFM relate the stress intensity factors to the stress filed in the crack tip ligament of the foam. Apart from considering only the tensile of struts, they also take into account the effect of bending moment (Figure 4).

Assuming that fracture of strut occurs when the maximum stress, for combined state of load bending and tensile, equals the ultimate tensile strength of the ligament material σ_{fs}, Choi and Sankar[31] relate the fracture toughness K_{IC} to the tensile strength of solid material, cell dimensions (l and h) and crack length (a) in the form of Equation 4:

$$K_{IC} = \sigma_{fs} \frac{h^2}{l} \sqrt{\frac{\pi}{2a}} \frac{1}{\left(1 + 2\frac{a}{h}\right)} \tag{4}$$

Similarly, the mode II fracture toughness was obtained considering the shear stress ahead of the crack tip[31] as follows:

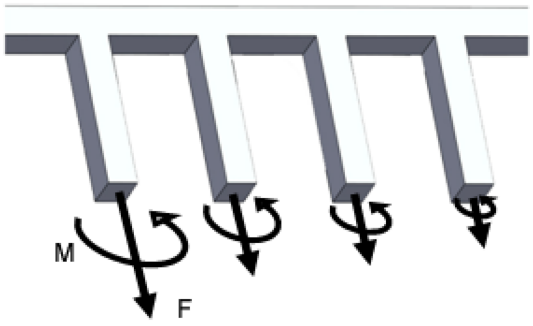

FIGURE 4 Forces and moments at the crack in foam, adapted from Choi and Sankar[31] [Colour figure can be viewed at wileyonlinelibrary.com]

$$K_{IIC} = \sigma_{fs} \frac{h^3}{3l^2} \sqrt{\frac{\pi}{2a}} \tag{5}$$

Choi and Lakes[32] proposed another model, which take into account the crack blunting and the nonsingular stress field ahead of the crack tip. The fracture toughness was obtained considering that the maximum stress in bending reaches the tensile strength of solid results:

$$K_{IC} = 0.20 \sigma_{fs} \sqrt{\pi l} \left(\frac{h}{l}\right)^2. \tag{6}$$

For regular tetrakaidecahedron cell packing, the relation between relative density and cell dimensions is

$$\left(\frac{\rho_f}{\rho_s}\right) = 1.06 \left(\frac{h}{l}\right)^2 \tag{7}$$

and the resulted fracture toughness is

$$\frac{K_{IC}}{\sigma_{fs}\sqrt{\pi l}} = 0.19 \left(\frac{\rho_f}{\rho_s}\right). \tag{8}$$

Considering a rectangular void shape of the strut cross section with the thickness h and void h_i (Figure 5), the fracture toughness could be expressed in the form[2]:

$$K_{IC} = C \sigma_{fs} \sqrt{\pi l} \left(\frac{\rho_f}{\rho_s}\right)^{3/2} \frac{1 + \left(\frac{h_i}{h}\right)^2}{\sqrt{1 - \left(\frac{h_i}{h}\right)^2}}. \tag{9}$$

Fan and Fang[33] presented a complex analysis of hollow structures. They concluded that the hollow-strut foams have superior mechanical properties compared with solid-strut foams for the same relative density. The hollow-strut foams are more damage tolerant than the solid-strut foam, because of their enlarged bending stiffness. The enhancements of stiffness, buckling strength, plastic collapse strength, brittle failure strength and fracture toughness were substantially increased according to their analysis. Three types of hollow struts were investigated with square, equilateral triangle and circular cross sections. Regarding the fracture toughness of hollow-strut foams, this is related to the ratio $f = h_i/h$, between length of inner side h_i and outer length h. The enhancement is 4.15 when the value of f is 0.9.

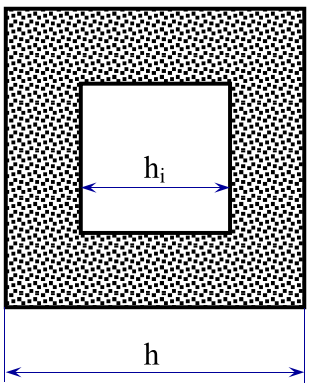

FIGURE 5 Strut with a rectangular void shape, adapted from Gibson and Ashby[2] [Colour figure can be viewed at wileyonlinelibrary.com]

Chen et al.[34] present a micromechanical analysis of cellular materials based on a strain gradient model. A generalized continuum model was applied considering the equivalence of strain energy at macroscale and microscale. The asymptotic field near crack and the full field solutions were obtained for different cell lattices: hexagonal, triangular and square. The fracture toughness was determined using the maximum tensile stress fracture criterion of cell wall. The fracture toughness is proportional with the cell thickness h and inversely proportional with square of cell size $l^{0.5}$ in the form:

$$K_{iC} = C_i \frac{\sigma_{fs} h}{\sqrt{l}} \tag{10}$$

where i corresponds to mode I and mode II of loading.

The values of C_i (i = I and II) for the considered cell lattices are shown in Table 1.

Lipperman et al.[35] considered a lattice model consisting of rigidly connected Euler beams, which can fail when the skin stress reaches a critical value. The fracture toughness for mode I and mode II was estimated, and the influence of the relative density was highlighted. The crack was modelled considering several broken beams. Four different cell topologies were defined as follows: kagome, triangular, square and hexagonal honeycombs (Figure 6), and the solution was determined analytically with discrete Fourier transform reducing the initial problem for unbounded domain to the analysis of a finite repetitive module in the transform space. For investigating the anisotropy of lattices, the results of the normalized fracture toughness $K_{IC}/\sigma_{fs}\sqrt{l}$ are shown in the form

TABLE 1 Values of C_I and C_{II} for the different cell lattices[34]

Cell shape	C_I	C_{II}
Hexagonal	1.8	0.77
Triangular	4.6	1.5
Square	1.4	0.068

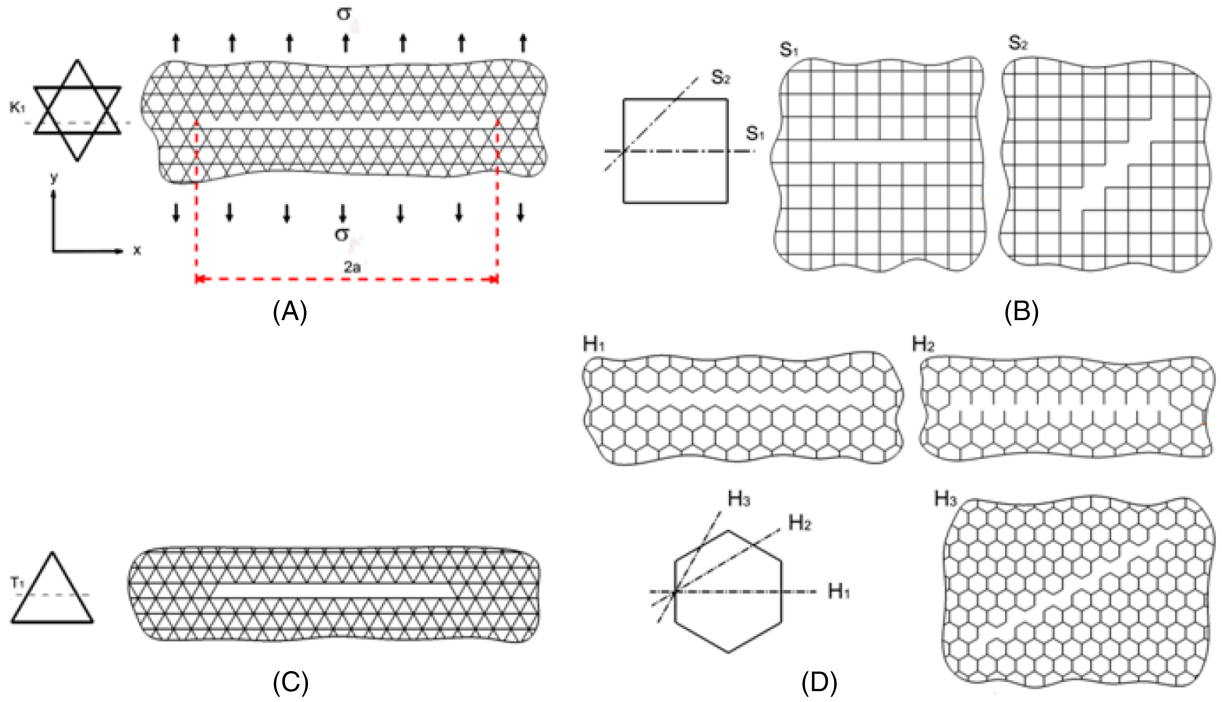

FIGURE 6 Lattice cracked models (A, kagome; B, square; C, triangular and D, hexagonal), adapted from Lipperman et al.[35] [Colour figure can be viewed at wileyonlinelibrary.com]

of polar diagrams, and quasi-isotropic fracture behaviour was observed for all investigated structures.

The variation of fracture toughness with relative density is investigated for different types of cell lattice. This is close to linear for kagome and triangular lattices and is in agreement with other published data.[2,34] The mode II fracture toughness is smaller than the mode I for almost all investigated cases.[35]

All the above micromechanical models relate the foam fracture toughness to the tensile strength of the solid material and microstructure parameters: cell length and relative density. The methodology assumes that the load is transmitted through the foam as a set of discrete forces and moments acting on cell struts. Different integration limits were used in order to determine the forces and moments. Singular[2,31] and nonsingular stress fields[32] in front of crack were considered. The fracture toughness was obtained by considering that the crack extents when the stress in the first strut in front of the crack reaches the tensile strength of the solid. When micromechanical models are used, the size effect regarding the variation of the tensile strength of the solid material σ_{fs} with strut size should be considered.[30] Huang and Gibson[29] proposed a statistical analysis based on Weibull distribution in order to show the effect of cell size on fracture toughness.

Choi and Lakes[32] relate the fracture toughness of foam K_{IC} to the fracture toughness of solid material K_{ICs}:

$$K_{ICs} = \sigma_{fs}\sqrt{\pi a}, \tag{11}$$

with a small defect in the bulk material, starting from a generalized expression of Equations 2a and 2b:

$$\frac{K_{IC}}{\sigma_{fs}\sqrt{\pi l}} = C\left(\frac{\rho_f}{\rho_s}\right)^{1+n} \tag{12}$$

with $n \geq 0$.

Substituting σ_{fS} between Equations 11 and 12, we obtain

$$\frac{K_{IC}}{\frac{K_{ICs}}{\sqrt{\pi a}}\sqrt{\pi l}} = C\left(\frac{\rho_f}{\rho_s}\right)^{1+n} \quad \text{yielding to}$$
$$\therefore \frac{K_{IC}}{\rho_f} = \frac{K_{ICs}}{\rho_s}\sqrt{\frac{l}{a}}C\left(\frac{\rho_f}{\rho_s}\right)^{n}. \tag{13}$$

More recently, Jelitto and Schneider[36,37] proposed some interesting geometric micromechanical models relating the fracture toughness K_{IC} of foams to the fracture mechanics of solid material K_{ICs}, considering three models:

- closed cell foams

$$\frac{K_{IC}}{K_{ICs}} = \left(1-P^{\frac{2}{3}}\right)^{\frac{1}{2}} \left(\frac{1-d}{-d^2+2d} + \frac{1}{-d+2+(1-d)^2 d^{-\frac{1}{2}}}\right)^{-\frac{1}{2}} \tag{14}$$

where $d = h/l$ represents a geometric parameter and $P = (1 - d)^3$ represents the porosity.

- open cell foams

$$\frac{K_{IC}}{K_{ICs}} = d^2 \left(\frac{-2d+3}{2d^2-4d+3}\right)^{\frac{1}{2}} \tag{15}$$

- open cell with discontinuities

$$\frac{K_{IC}}{K_{ICs}} = d\frac{\left(-2d^3+3d^2\right)^{m+\frac{1}{2}}}{\left(2d^2-4d+3\right)^{\frac{1}{2}}} \tag{16}$$

with m representing the amount of disconnected ligaments (Figure 7).

For the open cell and open cell with discontinuities structures, the relation between porosity and geometric parameter d is given by

$$d = \cos\left(\frac{2\pi - \cos^{-1}(2P-1)}{3}\right) + \frac{1}{2}$$

These micromechanical models were compared with different types of foams (polymeric and ceramic), and good correlation was observed. The model assumes that the toughness is proportional to the relative amount of substantial crack surface and that fracture occurs along the path with the minimum area of substantial crack face. It can be applied for any porosity between 0 and 1. An advantage of the models is that they are not dependent on the cell size.

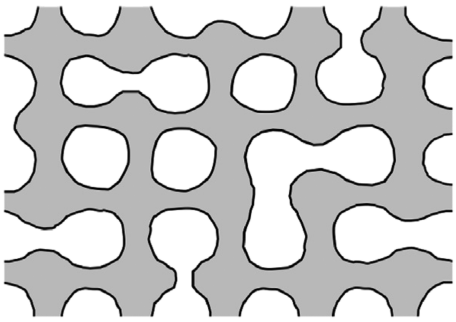

FIGURE 7 Typical cross section through the ligaments in a cell structure with disconnections, adapted from Jelitto and Schneider[36]

Fewer solutions are presented in the literature for mode III fracture toughness. Rivkin[38] proposed an analytical micromechanical model for a mode III crack in a lattice model using discrete Fourier transform and the solving the Wiener–Hopf equation. The expression of mode III fracture toughness is similar with Equations 2a and 2b:

$$K_{IIIC} = C\sigma_{fs}\sqrt{l}\left(\frac{\rho_f}{\rho_s}\right)^{1.5} \tag{17}$$

where C depends on the struts cross section and on the ratio between strut thickness h and cell size l.

A micromechanical model to investigate the influence of the cell size was presented by Huang and Lin[39] for mode II fracture toughness, considering two foams of the same density but with different cell size, in the form:

$$\frac{K_{IIC,1}}{K_{IIC,2}} = \left(\frac{l_1}{l_2}\right)^{\frac{1}{2}-\frac{2}{m}} \tag{18}$$

where $K_{IIC,1}$ and $K_{IIC,2}$ represent the fracture toughness of same density foam, but for different cell size l_1 and l_2. Fracture toughness of brittle foams increases with increasing cell size if $m > 6$, when $m < 6$ K_{IIC} decreases with increasing cell size, whereas if $m = 6$, there is no cell size effect.

Huang and Lin[39] also proposed a fracture criterion of brittle foam for mixed-mode loading, in the form of linear combination:

$$\frac{K_I}{K_{IC}} + \frac{K_{II}}{K_{IIC}} = 1. \tag{19}$$

At the end of this chapter, we can conclude that wide ranges of micromechanical models are available in the literature to predict the fracture toughness of polymeric foams considering different cell shapes (square, triangular, hexagonal and kagome). However, the use of these should be made with precaution without experimental validation.

3 | NUMERICAL PREDICTION OF FRACTURE TOUGHNESS FOR CELLULAR MATERIALS

Srivastava and Srivastava[40] presented a review of the polymeric foam modelling considering open and closed

cells, respectively regular and irregular cell topology. The available foam material models for finite element analysis (FEA) are reviewed, and the features of these models (like strain rate, damage, effect of temperature, failure, damage and anisotropy) are summarized. The material models have been validated through a series of tests such as tensile, compression, shear, hydrostatic stress, impact, drop test and indentation.

Finite element (FE) modelling methods are used to describe the mechanical behaviour and to predict the properties of cellular structures.[18,41–44]

In recent years, FE is increasingly applied to numerically investigate the fracture and damage of cellular materials.[31,45–47] FEA is particularly implemented for closed cell foams where the analytical formulations are more complex. Quintana-Alonso et al.[48] investigated the fracture toughness of cordierite square lattice.

Also, an FE-based method developed by Choi and Sankar[31] has been used by Wang[49] to study the fracture toughness of two types of foams: foams with rectangular prism unit cells, including homogeneous foams and functionally graded foams, and tetrakaidecahedral foams. He obtained the plain-strain fracture toughness of the foam by relating the fracture toughness to the tensile strength of the cell struts. In addition, he studied the effects of various geometric parameters that describe the cell. Two crack propagation criteria, one at the microscale and one at the macroscale, were used. The fracture toughness of brittle foam is calculated based on the stress intensity factor and the corresponding maximum tensile stress in the struts ahead of the crack. Fleck and Qiu[50] performed an FEA on hexagonal honeycomb, regular triangular honeycomb and Kagome lattice models using Euler Bernoulli beam elements with cubic interpolation functions, considering each beam with thickness t and length l. They present the prediction of fracture toughness related to the solid material in the form:

$$\frac{K_{IC}}{\sigma_{fs}\sqrt{\pi l}} = D\left(\frac{\rho_f}{\rho_s}\right)^d \tag{20}$$

where D is 0.212 (Kagome lattice), 0.5 (regular triangular honeycomb) and 0.8 (hexagonal honeycomb), whereas exponent d equals 2 for hexagonal honeycomb, 1 for regular triangular honeycomb and 0.5 for Kagome lattice loaded in mode I.

Christodoulou and Tan[51] present a study regarding the competing effects of cell regularity and relative density upon the fracture toughness under different loading modes of Voronoi honeycombs. To investigate the effects of the random cell topology, sufficiently large models of Voronoi tessellations were generated. The cell regularity was defined as nondimensional parameter Λ in the interval (0, 1] corresponding to complete irregular structure to a regular hexagonal honeycomb. A square FE mesh for each tessellation was created in ABAQUS/Standard software. Then periodic boundary conditions (BCs) were imposed on the lattice boundaries. The average fracture toughness of the lattices was fitted to the scaling law similarly with Equation 9. For mixed-mode loadings, the fracture loci were presented as K_{II}/K_{IC} versus K_I/K_{IC} (Figure 8) for different cell-regularity parameter Λ. The conclusion is that for pure mode I, fracture toughness of a lattice decreases as it becomes more irregular with an overall reduction of up to 25% for completely random lattices. The mode I fracture toughness of the lattices is more sensitive to cell topological variations than mode II.

Most of the micromechanical models considered the cell walls in a form of beams.[2,24,35,50] Linul and Marsavina[52] proposed a 2D solid FE model, based on rectangular cell geometry, similar with the cell topology of a 200-kg/m^3 PUR foam, for estimating the mode I and mode II fracture toughness. In order to obtain the fracture toughness, the model was loaded progressively, with a normal σ stress for mode I (Figure 9A), respectively with tangential stress τ for mode II (Figure 9D), up to the maximum normal stress in the first uncracked strut (positioned in front of the crack), reaches the fracture strength of solid material σ_{fs} (Figure 9B,E). The fracture toughness of cellular material was determined using Murakami[53] solution for crack (length 2a) in a plate (dimensions 2 W × 2H):

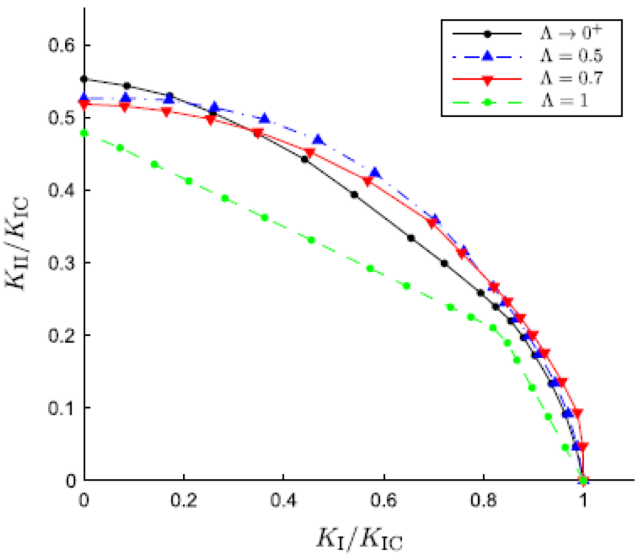

FIGURE 8 Fracture loci for regular and irregular Voronoi lattices, adapted from Christodoulou and Tan[51] [Colour figure can be viewed at wileyonlinelibrary.com]

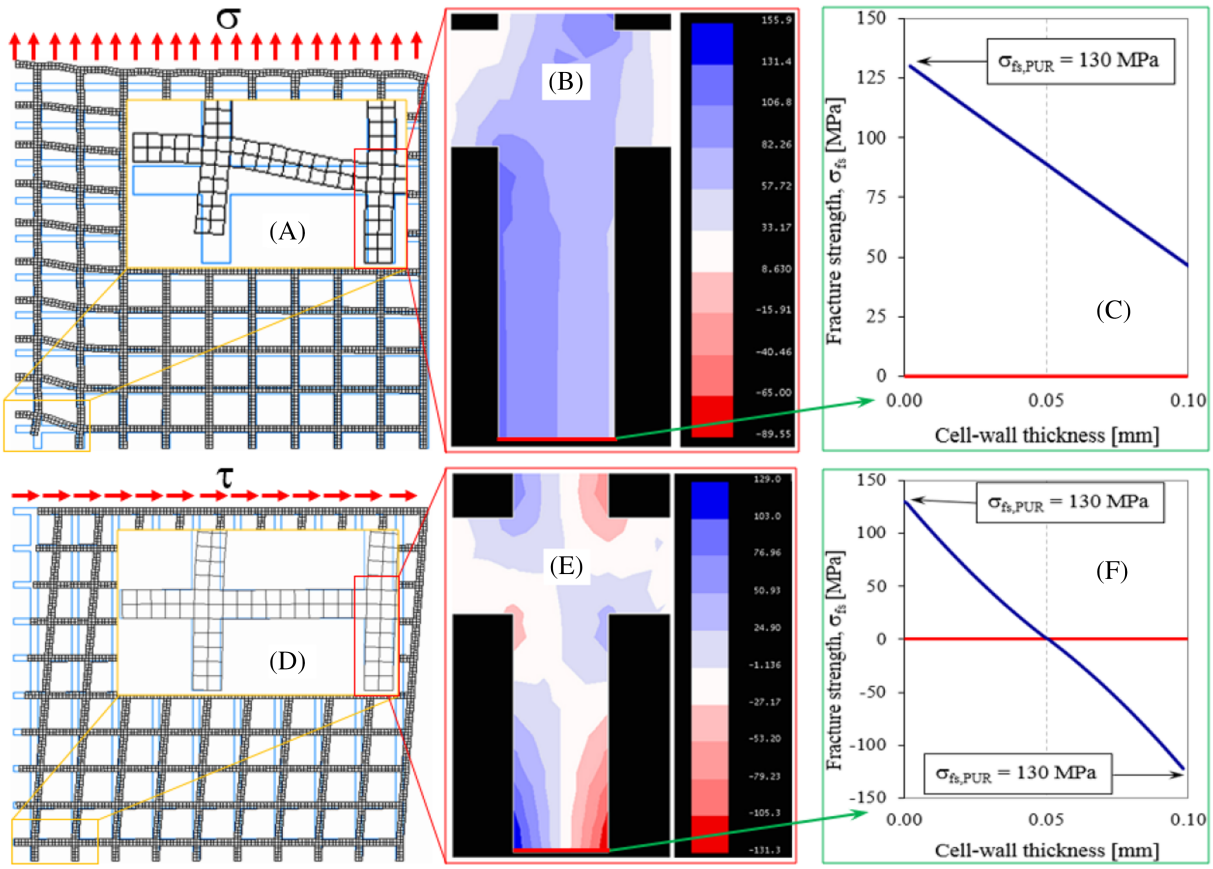

FIGURE 9 The 2D solid model from Linul and Marsavina[52] [Colour figure can be viewed at wileyonlinelibrary.com]

$$K_I = \sigma\sqrt{\pi a}\, F_I(a/W) = K_{IC}$$
$$K_{II} = \tau\sqrt{\pi a}\, F_{II}(a/W) = K_{IIC} \quad (21)$$

The mechanical characteristics of the solid polyurethane material were density, ρ_f = 1170 MPa; fracture strength, σ_{fs} = 130 MPa; Young's modulus, E = 1600 MPa and Poisson's ratio, ν = 0.4. The simulation was performed in Franc2D software, considering constant cell length, l = 0.52–0.60 mm, and variable strut thickness h (0.1, 0.05 and 0.02 mm), respectively constant strut thickness, h = 0.05 mm, and variable cell length l (0.55, 0.75 and 0.95 mm).

A convergence study was performed considering models from 4 × 4 cells to 10 × 10 cells for the same crack length. The results show small differences for mode I fracture toughness between 5 × 5 cells model and 10 × 10 cell model (Figure 10A). The effect of crack length was also investigated considering six different crack lengths: 1.4, 2.35, 3.3, 4.25, 5.2 and 6.15 mm (Figure 10B).

No influence of crack length on mode I (Figure 10) fracture toughness was observed. Figure 11 presents the values of fracture toughness for a PUR foam with 0.39 relative density and different cell numbers (36, 64, 100, 144, 196, 256 and 324) and crack lengths (0.85, 1.25, 2.05 and 2.65 mm) loaded in mode II. The mean value of K_{IIC} = 0.12 MPa m$^{0.5}$ with a scatter of ±0.02 MPa m$^{0.5}$. The relative differences in fracture toughness were small enough to conclude that the predicted fracture toughness could be considered independent on crack length (Figures 10 and 11).

The advantage of this model is that fully describe the stress field in the solid struts. The stress distribution in the first uncracked strut shows a complex stress (bending and tension) for mode I loading (Figure 9C), whereas for mode II loading (Figure 9F), a pure bending occurs. The comparison with other micromechanical models and experimental data of fracture toughness validates the solid 2D micromechanical model.

Based on real microstructures of the PUR foams, Linul et al.[54] extended the previous study (square cells) considering other types of PUR foams cell topologies, such as hexagonal and circular cells (Figure 12).

Different relative densities were considered for the three investigated cell topologies. The results for mode I fracture toughness are shown in Figure 13. It could be observed a linear correlation between K_{IC} and relative density, and the fracture toughness for hexagonal cells is the highest, whereas minimum values were obtained for square cells.

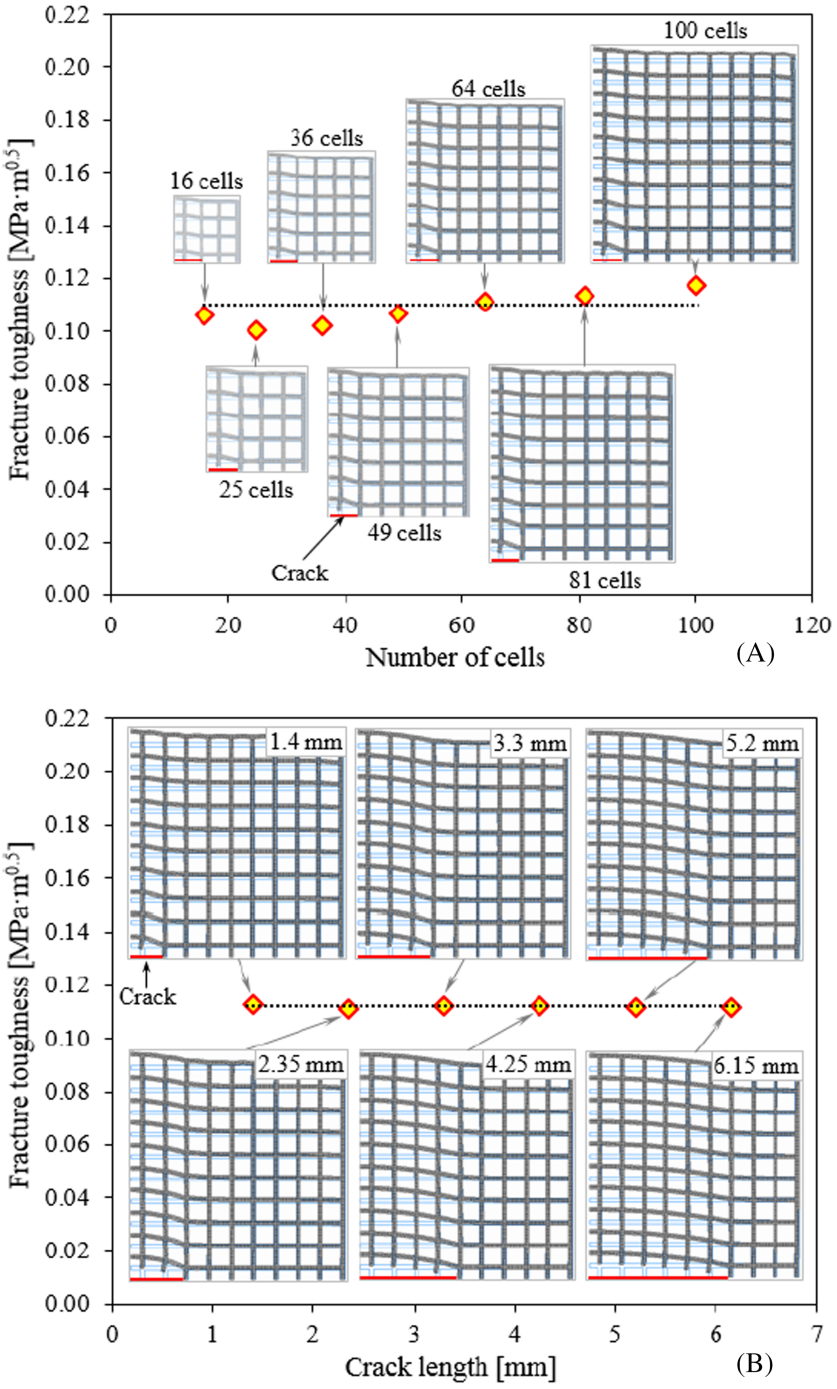

FIGURE 10 Effect of the number of cells (A) and crack length (B) on K_{IC} values [Colour figure can be viewed at wileyonlinelibrary.com]

Choi and Sankar[31] (Figure 14) presented a comparison between a solid 3D model and a beam model to predict fracture toughness of carbon foam. They obtained good agreement between the predicted values and experimental values.

Thiyagasundaram et al.[55] developed a 3D FE micromechanical model based on tetrakaidecahedral unit cell. The foam was modelled as homogeneous orthotropic material in the outer region, whereas in the crack dominant zone, a beam structure having a tetrakaidecahedral unit cell and a triangular cross section of the struts (Figure 15). The FE was obtained by repeating unit cell with strut length $l = 1$ mm and cross-section dimension $h = 0.06$ mm resulting a relative density $\rho_f/\rho_s = 0.00165$. The solid material from the cell struts has density of $\rho_s = 1650$ kg/m^3, Young's modulus, $E_s = 23.42$ GPa; Poisson's ratio, $v_s = 0.33$ and tensile strength, $\sigma_{fs} = 685.5$ MPa. The crack was introduced by removing the cells along the crack length. The imposed BCs were the displacements near the crack tip for homogeneous

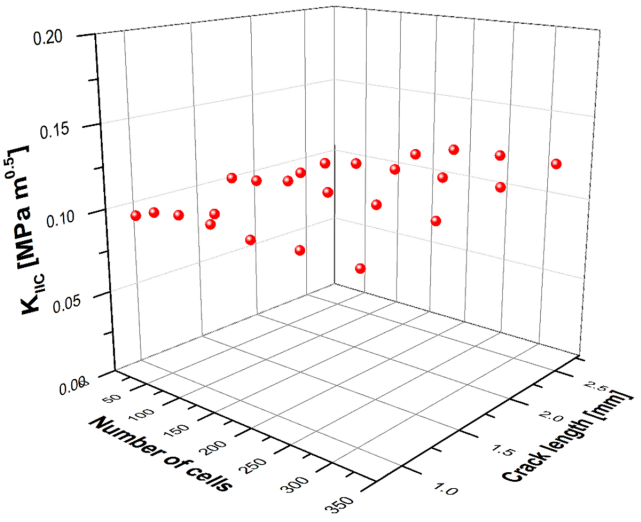

FIGURE 11 Effect of the number of cells and crack length on K_{IIC} values [Colour figure can be viewed at wileyonlinelibrary.com]

orthotropic material. The predicted fracture toughness results converge as the size of micromechanical model increased above 700 cells.

Wang,[49] in order to determine the plane strain fracture toughness, used a tetrakaidecahedral unit cell having 14-sided polyhedron with six square and eight hexagonal faces. The normalized fracture toughness of tetrakaidecahedral foam mainly depends on its relative density and is expressed in a similar relation to Equation 9. The relative density depends on the strut length l and dimension of strut (considered as equilateral triangle) h by $\frac{\rho_f}{\rho_s} = 0.4593\left(\frac{h}{l}\right)^2$.

The variation of mode I and mode II fracture toughness versus relative density for $l = 2$ mm is shown in Figure 16.

Arakere et al.[47] investigating the BX-265 foam insulation material, with 35.2 kg/m^3 density, used a solid 3D for middle tension specimen. The specimen was modelled as transversally isotropic linear elastic solid, and different crack orientations were defined for modes I, II and III combinations. Fracture toughness was estimated equating with the stress intensity factor obtained with the fracture load from tests.

Settgast et al.[56] modelled reticulated Kelvin open cell containing sharp edges cavities using 3D FE method. The interaction integral was employed to compute the local stress intensity factors under multiaxial loading. Using a homogenization approach, a criterion for brittle failure based on the effective stress state is presented.

Investigating the fracture behaviour of rigid closed-cell PVC foam Divinycell HT-90 (density 90 kg/m^3), Rizov and Mladensky[57] presented experimental and numerical results. The fracture toughness was calculated based on nodal displacement correlation from the near crack zone. A fracture toughness value of

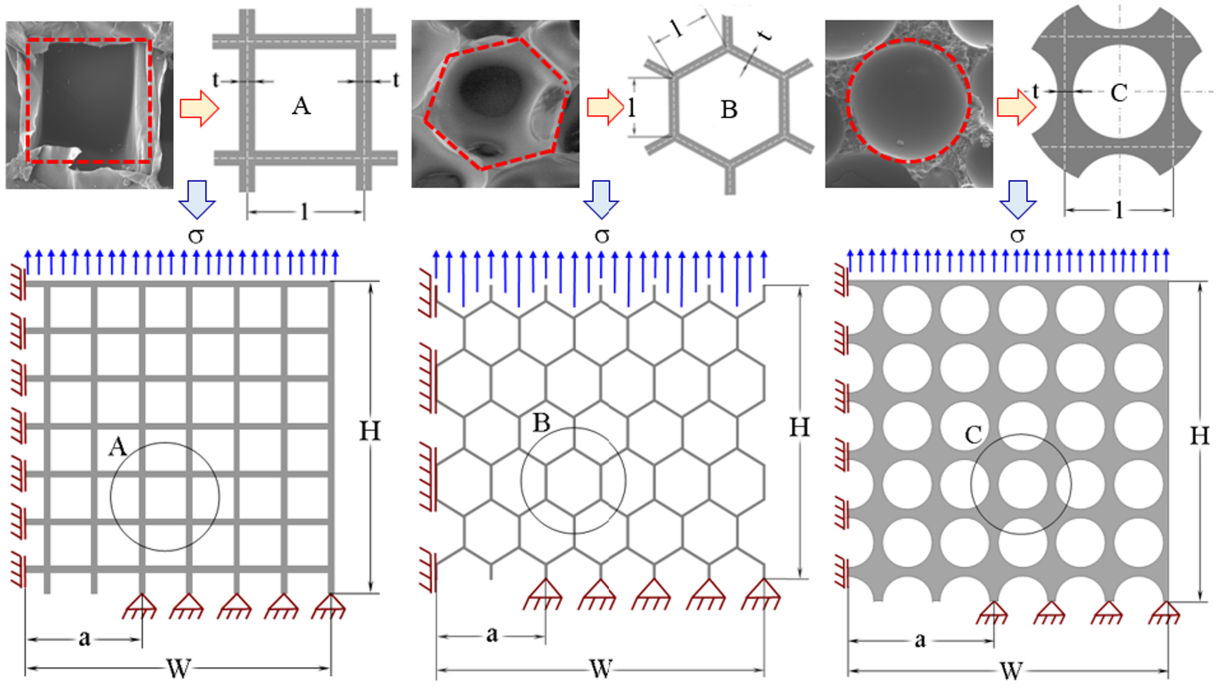

(A) square cells (B) hexagonal cells (C) circular cells

FIGURE 12 The 2D models dimensions and boundary conditions for square, honeycomb and circular cells[54] [Colour figure can be viewed at wileyonlinelibrary.com]

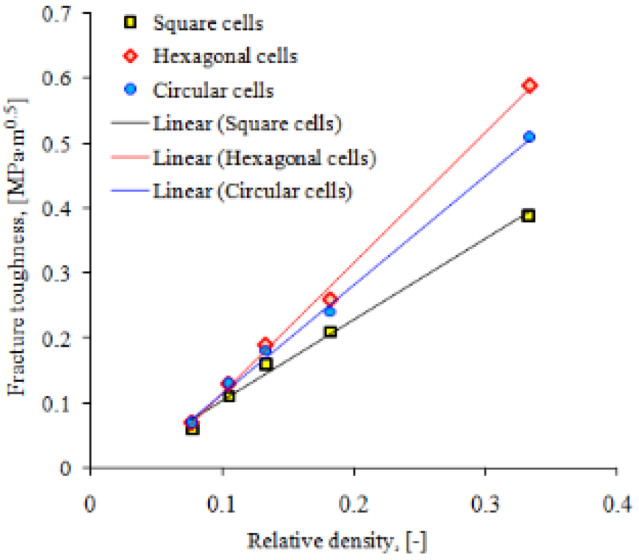

FIGURE 13 Fracture toughness versus relative density[54]
[Colour figure can be viewed at wileyonlinelibrary.com]

K_{IC} = 0.222 MPa $m^{0.5}$ was found, and it was concluded that the three-dimensional model represents an accurate tool for analysing the mechanical response of the compact tension (CT) specimen.

The FE micromechanical models offer an alternative to analytical micromechanical models. Most of the numerical investigations relate the fracture properties to solid material of the foam, relative density, cell size, cell shape, cellular topology, cell walls thickness and distributions of solids between struts and faces. Two and three-dimensional foam models were considered, with cells of different shapes (beams, 2D and 3D solids). Both mode I and II fracture toughness were predicted.

4 | EXPERIMENTAL DETERMINATION OF MODE I FRACTURE TOUGHNESS

The testing methods for mechanical characterization of polymeric materials are described in Landrock,[58] Brown,[59,60] Ward and Sweeney[61] and Park et al.[62] However, up to now, there are no standards for fracture toughness determination of polymeric foams. Most of the experiments were performed using the plane strain fracture toughness of plastic materials procedure from ASTM D5045-99.[63]

4.1 | Types of specimens

Single-edge notched bending (SENB) specimens (Figure 17A) and CT specimens (Figure 17B) are recommended because they exhibit a predominantly bending stress state, which allows smaller specimen sizes to achieve plane strain conditions. If the material is supplied in the form of a sheet, the specimen thickness, B, should be identical with the sheet thickness. The plain strain condition could be achieved only if specimen thickness B is big enough and the ligament in the crack area ($W - a$) is sufficient to avoid excessive plasticity. The introduction of a crack in the specimen is possible by machining a sharp notch. Subsequently, one can initiate a natural crack by inserting a fresh razor blade and tapping. If a natural crack cannot be successfully initiated by tapping, a sufficiently sharp crack can alternatively be generated by sliding or sawing with a new razor blade across the notch root.

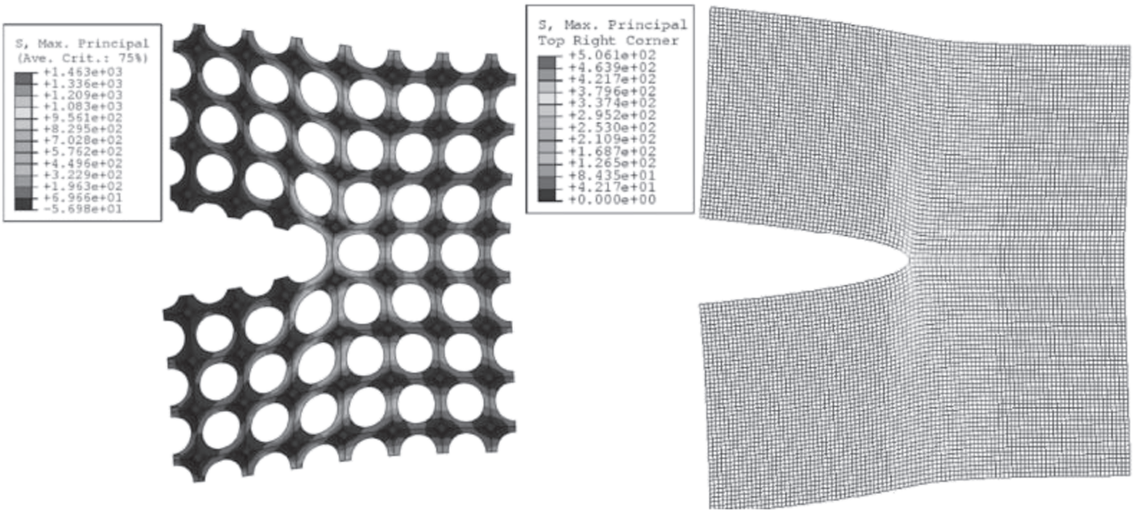

(A) Solid model (B) Beam model

FIGURE 14 Finite element micromechanical models[31]

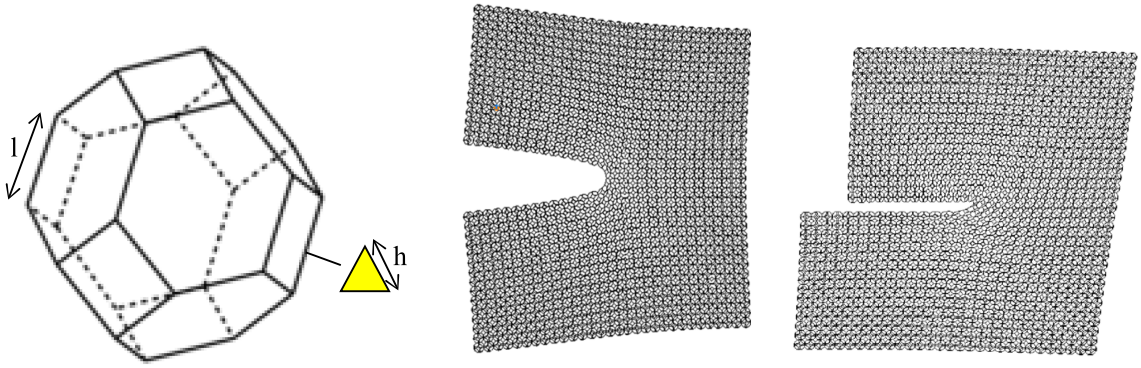

FIGURE 15 The tetrakaidecahedral unit cell and the cross section of a strut, adapted from Thiyagasundaram et al.[55] [Colour figure can be viewed at wileyonlinelibrary.com]

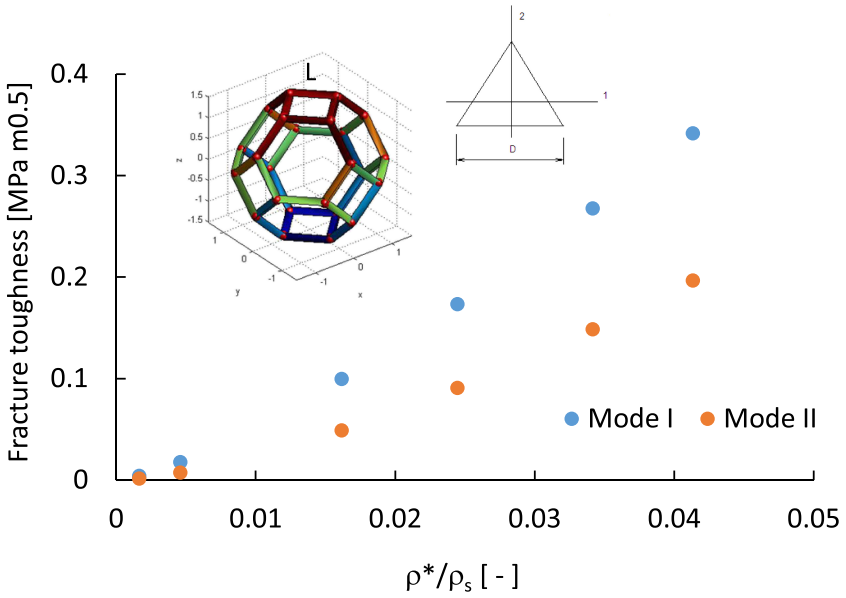

FIGURE 16 The fracture toughness versus relative density, adapted from Wang[49] [Colour figure can be viewed at wileyonlinelibrary.com]

Fowlkes[25] performed one of the first experimental investigation on fracture toughness of PUR foams with a density of 88 kg/m^3. He considered different types of specimens: middle cracked (MC) specimen (Figure 17C), double-edge crack specimen, single-edge crack (SEC) specimen (Figure 17D) and double cantilever beam (DCB) (Figure 17F) and determined the critical energy release rate G_{IC}. The results obtained on DCB were 0.22 kJ/m^2, and on the other specimens, 0.193 ± 10% kJ/m^2. He also highlighted that the fracture toughness results do not depend on specimen type, representing a material property. On the contrary, Poapongsakorn and Carlsson[64] using SENB specimens showed that symmetric four point-bending (FPB) loading (Figure 17A) gives a fracture toughness two times higher compared with loading in three-point bend (TPB) (Figure 17A) configuration, because of indentation that occurs in the cracked cross-section area, reducing the ligament size.

Figure 17 presents some of the most used specimens in fracture toughness tests of polymeric foams.

Table 2 summarizes the fracture toughness K_{IC} experimental results for different polymeric foams, different densities and specimen configurations from literature.

Because of the diversity of polymeric foams, specimen types and dimensions are hard to compare with those values of mode I fracture toughness. However, some correlations could be made. Most of the fracture tests were performed on one type of specimen SENB. Marsavina et al.[75,76] presented results of PUR foam fracture toughness using different types of specimens. Their results for three different densities and four types of specimens and loading configurations are summarized in Figure 18. It could be seen that the mode I fracture toughness values are similar, with the exception of those obtained on SEC specimens, which are higher with 12% (density 300 kg/m^3) to 32% (density 100 kg/m^3) than those obtained using SENB specimens loaded on TPB.

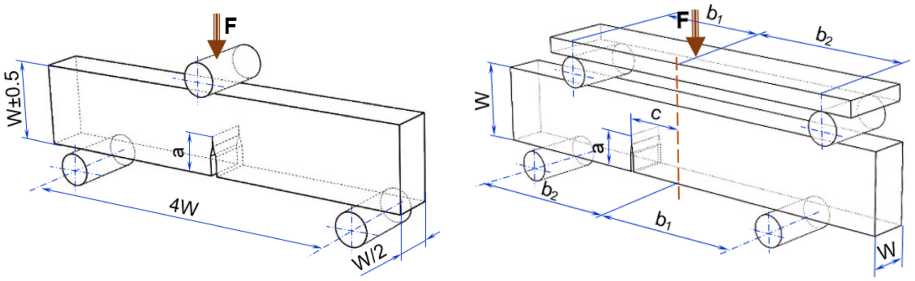

loaded in three point bending (TPB) loaded in four point bending (FPB)

(A) Single Edge Notch Bend (SENB) specimen

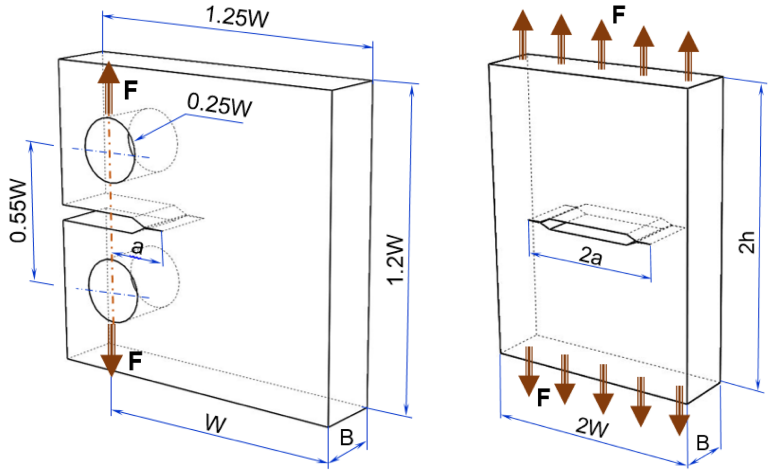

(B) Compact Tension (CT) specimen (C) Middle Crack (MC) specimen

FIGURE 17 Types of specimens for fracture toughness tests [Colour figure can be viewed at wileyonlinelibrary.com]

4.2 | Influence of solid material

Kabir et al.[67] compared the fracture toughness of PVC and PUR foams of 260-kg/m^3 density and highlighted that $K_{IC,PVC}$ is 2.2 times higher than those obtained for PUR $K_{IC,PUR}$. Similar results could be seen if we compare the foams with 100-kg/m^3 density for H100 PVC foam (Viana and Carlsson[66]) and PUR 100 (Marsavina et al.[75]) (Table 2). All these results together with the foam microstructure are shown in Figure 19. This figure could be explained on one hand on the higher fracture toughness of solid material PVC $K_{IC,PVCs}$ = 2.45 MPa m$^{0.5}$ in comparison with PUR $K_{IC,PURs}$ = 0.35 MPa m$^{0.5}$. In addition, the topology of the compared foams is different: PVC foams have a hexagonal structure, whereas the PUR ones have a spherical microstructure (Figure 19).

Bureau and Kumar[78] investigated the fracture toughness of microcellular polycarbonate foam with relative density between 0.7 (density 830 kg/m^3) and 0.9 (density 1073 kg/m^3) manufactured by solid-state foam and obtained fracture toughness values between 2.6 ± 0.1 and 4.3 ± 0.3 MPa m$^{0.5}$.

Saenz et al.[79] experimentally determined the fracture toughness G_{IC} (in kJ/m^2) of PVC and PES foam using SENB and DCB specimens. Their results are shown in Table 3.

It also could be observed that at almost the same density (54 kg/m^3), the fracture toughness of PES-P50 foam is 52% higher compared with the corresponding density of PVC foam (H60). The authors explain that the cross-inked PVC foams failed in a linear elastic brittle manner, whereas the thermoplastic PES foams displayed much more ductility and substantially higher fracture toughness. The differences on fracture toughness for the same PVC foam density obtained using SENB, respectively DCB specimens are due to the different loading speeds and specimen orientation. The SENB specimens were cut out-of-plane and tested at 12.7 mm/min, whereas the DCB specimens were cut in-

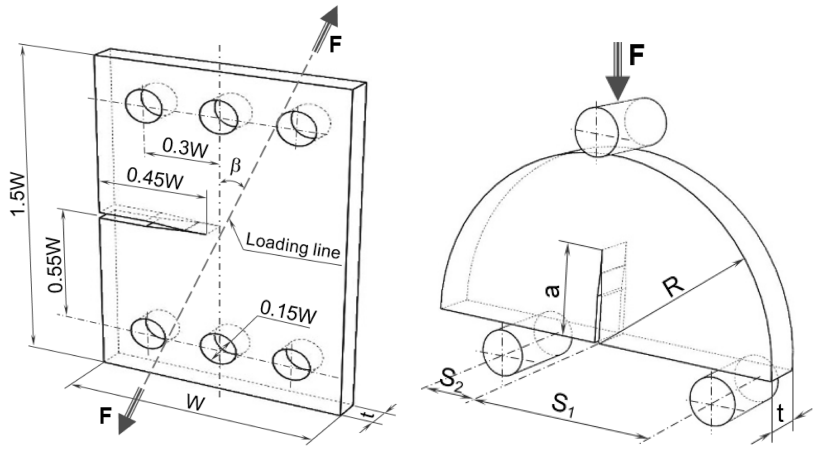

(D) Single Edge Crack (SEC) specimen (E) Asymmetric Semi Circular Bend (ASCB) specimen

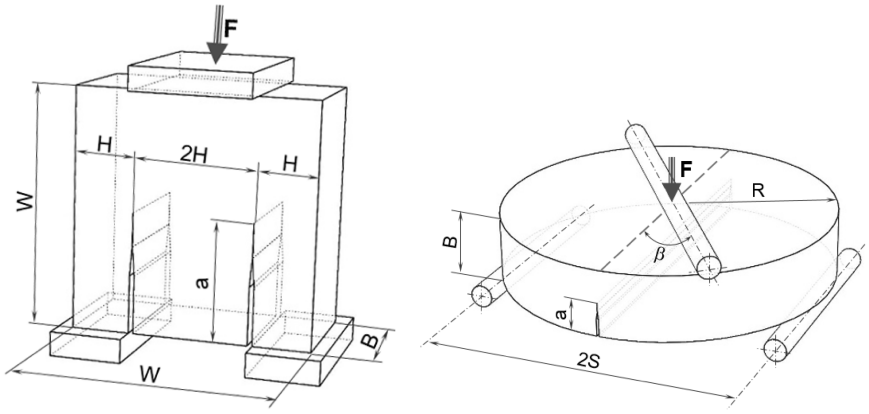

(F) Compact Shear (CS) specimen (G) Edge Notch Bend Disc (ENDB) specimen

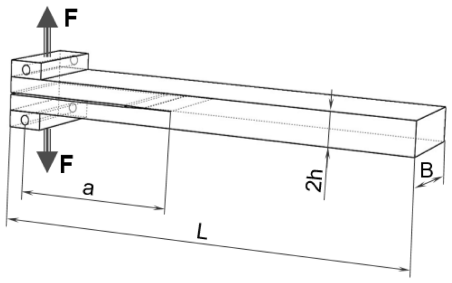

f. Double Cantilever Beam (DCB) specimen

FIGURE 17 (Continued)

plane and tested at 1.27 mm/min. Similar results for G_{IC} of H100 PVC foam obtained using DCB specimens with different core thicknesses (from 3.18 to 40.6 mm) were obtained by Matteson et al.[80] and Shivakumar et al.,[81] and the G_{IC} values range between 1.02 and 0.88 kJ/m^2.

Saenz et al.[82,83] also investigated the propagation of crack in PVC and PES foams using SEC specimens loaded in tensile and concluded that for both foams, the cells failed in a stretching mode of deformation.

4.3 | Influence of loading speed

The influence of density and loading speed for PVC foams was presented by Kabir et al.[67] The fracture toughness increases with loading speed, and this increase is lower for the high-density foam: 22% for 75-kg/m^3 density, respectively 18% for 260-kg/m^3 density, considering a 100 times increase of loading speed (Figure 20A). This increase appears only for loading in flow direction, whereas in the rise direction, the loading speed has

TABLE 2 Fracture toughness K_{IC} values of polymeric foams

Foam type/grade	Density ρ_f (kg/m^3)	Specimen type	Crack length a (mm)	Fracture toughness K_{IC} (MPa m$^{0.5}$)	References
PUR	35	SENB/TPB	Not available	0.010	McIntyre and Anderton[65]
PUR	55	SENB/TPB	Not available	0.024	
PUR	79	SENB/TPB	Not available	0.035	
PUR	88	SENB/TPB	Not available	0.039	
PUR	97	SENB/TPB	Not available	0.038	
PUR	112	SENB/TPB	Not available	0.054	
PUR	120	SENB/TPB	Not available	0.046	
PUR	135	SENB/TPB	Not available	0.067	
PUR	155	SENB/TPB	Not available	0.085	
PUR	158	SENB/TPB	Not available	0.087	
PUR	160	SENB/TPB	Not available	0.097	
PUR	222	SENB/TPB	Not available	0.107	
PUR	280	SENB/TPB	Not available	0.202	
PUR	356	SENB/TPB	Not available	0.238	
PUR	358	SENB/TPB	Not available	0.243	
PVC/H30	36	SENB/TPB	19.5	0.064	Viana and Carlsson[66]
PVC/H80	80	SENB/TPB	18.5	0.117	
PVC/H100	100	SENB/TPB	27.6	0.168	
PVC/H200	200	SENB/TPB	24.0	0.370	
PVC/R400	400	SENB/TPB	13.5	0.450	
PVC/R75	75	SENB/TPB	$0.40 < a/W < 0.60$	0.09	Kabir et al.[67]
PVC/H130	130	SENB/TPB	$0.40 < a/W < 0.60$	0.28	
PVC/HD130	200	SENB/TPB	$0.40 < a/W < 0.60$	0.47	
PVC/R260	260	SENB/TPB	$0.40 < a/W < 0.60$	0.63	
PUR/240	240	SENB/TPB	$0.40 < a/W < 0.60$	0.32	
PUR	40	SENB/TPB	12.0	0.034	Marsavina and Linul[68]
PUR	80	SENB/TPB	12.0	0.058	
PUR	120	SENB/TPB	12.0	0.120	
PUR	140	SENB/TPB	12.0	0.153	
PUR	145	SENB/TPB	12.0	0.210	
PUR	200	SENB/TPB	12.0	0.390	
PUR	300	SENB/TPB	12.0	0.590	
PVC/H45	46.1	SENB/TPB	$0.45 < a/W < 0.55$	0.05	Poapongsakorn and Carlsson[64]
PVC/H60	60.4	SENB/TPB	$0.45 < a/W < 0.55$	0.07	
PVC/H100	100	SENB/TPB	$0.45 < a/W < 0.55$	0.13	
PVC/H130	121	SENB/TPB	$0.45 < a/W < 0.55$	0.16	
PVC/H200	208	SENB/TPB	$0.45 < a/W < 0.55$	0.35	
PVC/H45	46.1	SENB/FPB	$0.45 < a/W < 0.55$	0.09	
PVC/H60	60.4	SENB/FPB	$0.45 < a/W < 0.55$	0.13	
PVC/H100	100	SENB/FPB	$0.45 < a/W < 0.55$	0.25	
PVC/H130	121	SENB/FPB	$0.45 < a/W < 0.55$	0.31	

(Continues)

TABLE 2 (Continued)

Foam type/grade	Density ρ_f (kg/m^3)	Specimen type	Crack length a (mm)	Fracture toughness K_{IC} (MPa m$^{0.5}$)	References
PVC/H200	208	SENB/FPB	0.45 < a/W < 0.55	0.63	
PMI/WF51	52	SENB/TPB	0.20 < a/W < 0.80	0.08	Burman[69]
PVC/H100	100	SENB/TPB	0.20 < a/W < 0.80	0.21	
PIR	34	CT	Not available	0.010	Andersons et al.[70]
PIR	41	CT	Not available	0.012	
PIR	53	CT	Not available	0.017	
PIR	64	CT	Not available	0.019	
PUR	32	CT	Not available	0.022	
PUR	51	CT	Not available	0.038	
PUR	77	CT	Not available	0.055	
PUR	84	CT	Not available	0.058	
PUR	320	SENB	10.2	0.215	Jin et al.[71]
Styrene/A800	150	SENB	Not available	0.334	Kidane[72]
Styrene/A1200	210	SENB	Not available	0.435	
PUR	100	SENB/FPB	12.0	0.075	Apostol et al.[73,74]
PUR	145	SENB/FPB	12.0	0.100	
PUR	300	SENB/FPB	12.0	0.369	
PUR	100	ASCB	20.0	0.087	Marsavina et al.[75]
PUR	145	ASCB	20.0	0.131	
PUR	300	ASCB	20.0	0.372	
PUR	100	SEC	33.75	0.131	Marsavina et al.[76]
PUR	145	SEC	33.75	0.140	
PUR	300	SEC	33.75	0.421	
PUR	100	ENDB	15.0	0.091	Aliha et al.[77]
PUR	145	ENDB	15.0	0.112	
PUR	300	ENDB	12.5	0.344	

practically no influence. Poapongsakorn and Carlsson[64] investigated the influence of crosshead rate and cell size for three different 60-kg/m^3 PVC foams (two normal H60, H60N and one with large cells H60L) using SENB specimen loaded in FPB. Three different cross speed rates were considered 0.254, 1.27 and 12.7 mm/min. The results show that crosshead rate does not have significant influence on the fracture toughness for foams with normal cells H60 and H60N. The H60L foam with large cells tested at a low rate of 0.245 mm/min displayed low fracture toughness values.

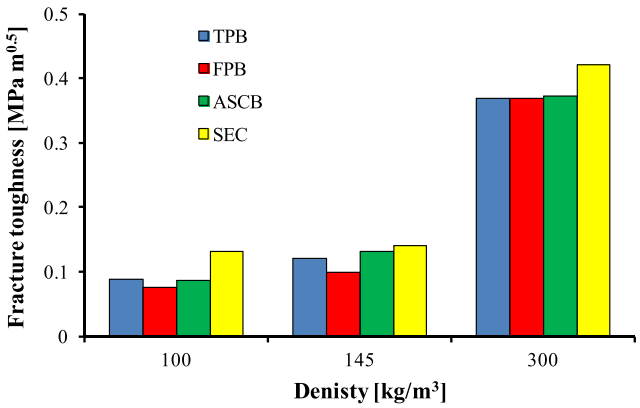

FIGURE 18 Influence of specimen type on fracture toughness[75,76] [Colour figure can be viewed at wileyonlinelibrary.com]

For PUR foam with 140-kg/m^3 density, the fracture toughness decreases with 11% when loading speed increases 200 times.[68] The different tendency could be again explained on the topology of the cells.

4.4 | Influence of foam anisotropy

Cellular materials and particularly foams are often anisotropic, and their properties depend on the direction in

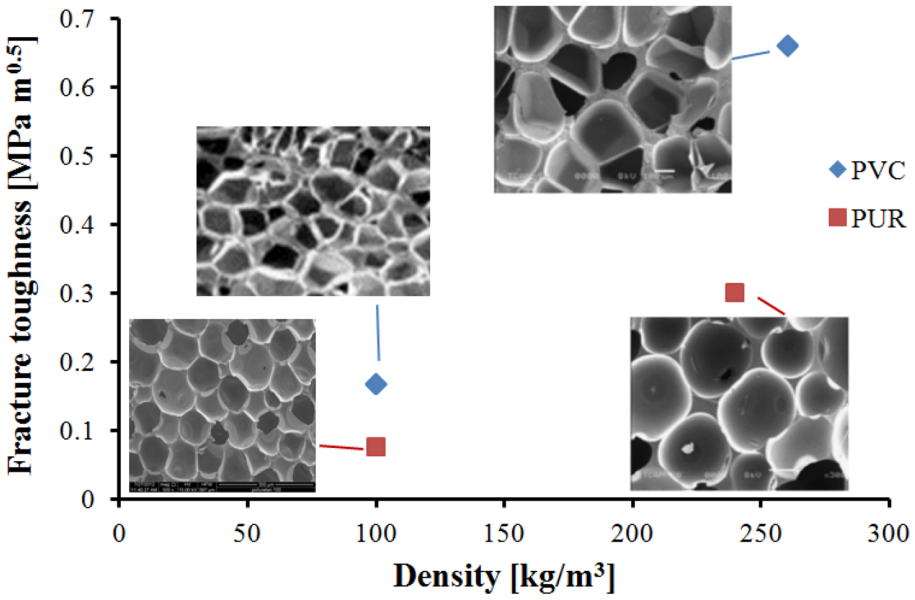

FIGURE 19 Influence of solid material on fracture toughness [Colour figure can be viewed at wileyonlinelibrary.com]

TABLE 3 Fracture toughness of PVC and PES foams[79]

Foam type		Density (kg/m³)	Fracture toughness G_{IC} (kJ/m²) SENB	DCB
PVC	H45	48.3 ± 0.39	0.11 ± 0.01	0.24 ± 0.03
	H60	54.9 ± 0.63	0.24 ± 0.01	0.38 ± 0.04
	H100	107.0 ± 1.79	0.43 ± 0.04	0.89 ± 0.05
PES	P50	54.3 ± 0.84	-	0.58 ± 0.15
	P90	86.0 ± 4.04	-	0.72 ± 0.08
	F130	125.0 ± 4.53	-	1.53 ± 0.30

which they were measured.[2] Huber and Gibson[84] proposed scaling relations for mode I fracture toughness of brittle anisotropic foams, using rectangular parallelepiped unit cell of foams and brittle fracture in bending as the crack growth mechanism. The fracture toughness of an anisotropic foam depends on the direction in which the crack propagates. The anisotropy is influenced by the cell dimensions and topology, which could be identified for three directions: two in the flow direction, in-plane (1), (2) and one out-of-plane corresponding to rise direction (3) (Figure 21).

The average geometrical anisotropy factor defined as follows[70]:

$$Q = \frac{1}{N}\sum_{i=1}^{N}\frac{l_{R,i}}{l_{F,i}} \tag{22}$$

is based on the geometrical dimensions h (cell dimension in the rise direction) and l (cell dimension in the flow direction), with N the number of cells for a given sample. They correlate the ratio between fracture toughness on different direction to the ratio of cell dimensions $Q = l_{\text{rise}}/l_{\text{flow}}$:

$$\frac{(K_{IC})_i}{(K_{IC})_j} = Q^N \tag{23}$$

with $i, j = 1, 2, 3$ direction, $N = 0.5, 1, 1.5$.

Figure 22 presents the analytical predictions of $K_{IC\_\text{rise}}/K_{IC\_\text{flow}}$ versus h/l given by Equation 23, together with the experimental results for

- SENB specimens (yellow circle for 100-kg/m³ density, blue circle for 145-kg/m³ density and black circle for 300-kg/m³ density);
- ASCB specimens for 100-kg/m³ density (yellow square) and 145-kg/m³ density (blue square) obtained for PUR foams[75,76];
- MT specimens of 35.2-kg/m³ BX-265 PUR foam[47];
- SENB specimens from PVC foam of density 130 kg/m³.[67]

It could be observed that the ratio $K_{IC\_\text{rise}}/K_{IC\_\text{flow}}$ is higher than 1, and the anisotropy decreases with increasing the foam density.

Ganpatye and Kinra,[85] investigating the fracture toughness of low-density (35.2 kg/m³) polyurethane closed-cell foam BX-265, used for insulation of external tanks of space shuttles, highlighted similar anisotropy effect $(K_{IC})_{32}/(K_{IC})_{21} = 1.43$, where $(K_{IC})_{32} = 0.029$ MPa m$^{0.5}$ and $(K_{IC})_{21} = 0.020$ MPa m$^{0.5}$.

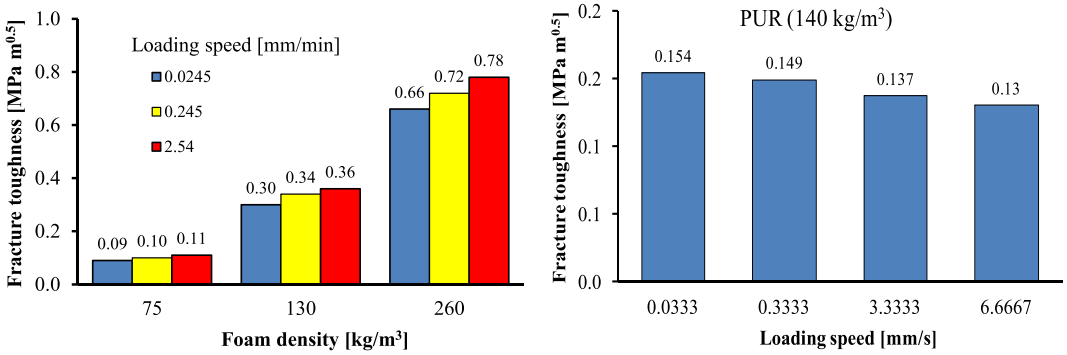

(A) PVC foam[64] (B) PUR foam[68]

FIGURE 20 Influence of loading speed on fracture toughness [Colour figure can be viewed at wileyonlinelibrary.com]

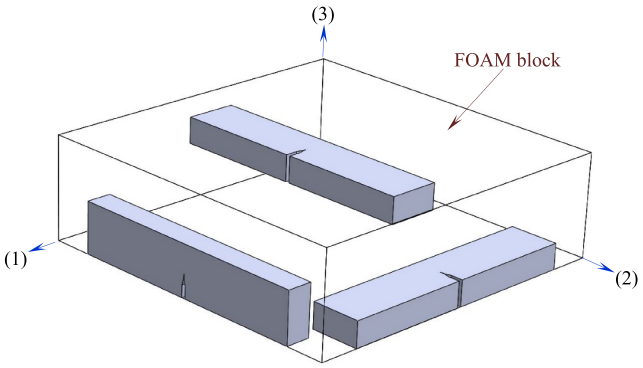

FIGURE 21 Single-edge notched bending specimens orientation [Colour figure can be viewed at wileyonlinelibrary.com]

4.5 | Influence of testing temperature

The main physical and mechanical properties of different polymeric foams have been investigated in detail by different researchers under low temperatures (between 0°C and −196°C), especially at cryogenic temperature.[86–92] On the other hand, the literature presents very limited studies regarding the determination of fracture toughness values under extreme temperature conditions. Knudsen[93] presents a summary of tests performed at NASA for BX-265 foam insulation at room temperature and −178°C, using different types of specimens (SENB, MC and CT).

Fracture mechanics experimental tests of cellular materials under low- or high-temperature conditions are very difficult to perform, both due to the clamping devices and to the cooling/heating installations.

Using an insulation chamber, Yu et al.[94] investigated the K_{IC} of the neat (unreinforced) and chopped glass fibre (CGF) reinforced polyurethane foams (70 kg/m^3) at cryogenic temperature. The authors adopted the eccentrically loaded, CT specimen, and they used CGF lengths of 7-mm length and different percentages. The experimental tests were performed at −150°C, using a CGF length of 7 mm and different percentages of CGF (2.5, 5.0, 7.5 and 10.0 wt%). The authors observed that the K_{IC} increased as the weight percentages of the CGF were increased. More precisely, the K_{IC} of the CGF reinforced PUR foam increased by 360% at −150°C with the reinforcement of 10 wt% of CGF. Furthermore, because of the increase of

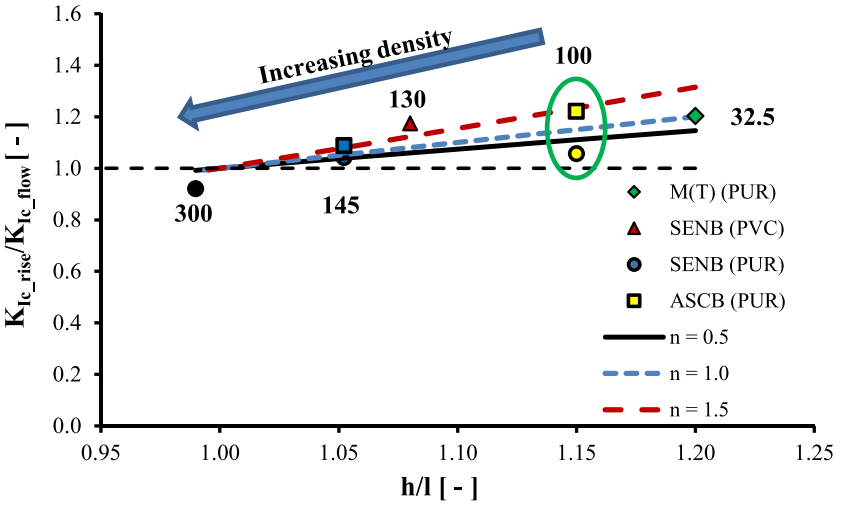

FIGURE 22 Influence of foam anisotropy [Colour figure can be viewed at wileyonlinelibrary.com]

brittleness of PUR foam, they observed that the K_{IC} of the neat PUR foam decreased at the cryogenic temperature compared with that of the room temperature. However, the K_{IC} of the CGF reinforced PUR foams increased more at −150°C than that at the room temperature (by about 20%). According to their SEM images, this phenomenon is associated with the bridging effect that will increase the intermolecular force of the polyurethane polymer during cryogenic temperature tests. When the crack tip propagates, some bridged CGFs will be pulled out from the PUR foam, which will dissipate much the strain energy stored in the reinforced foam. The dissipation of strain energy will increase the K_{IC} of the CGF reinforced foam.[95]

Recently, Linul et al.[96] determined the quasi-static K_{IC} of rigid PUR foams under cryogenic temperature by using SENB specimens. The authors investigated both the influence of foam density (100, 145 and 300 kg/m^3) and foam anisotropy (in-plane and out-of-plane loading direction) at −196°C (the specimens being totally immersed in liquid nitrogen). They found that the cryogenic temperature in-plane K_{IC} values are lower than the out-of-plane ones with about 16%, especially for low densities, whereas for high densities, the K_{IC} difference is below 6%. Moreover, regardless of foam density and loading direction, all PUR foam specimens highlighted a significant increase in K_{IC} at −196°C, compared with room temperature (i.e., 30%–39% for 100 and 145 kg/m^3, and 15% for 300 kg/m^3) (Figure 23). It seems that because of the different test parameters (e.g., different cooling systems of the specimens, different testing temperature, different test type and different specimen shape) and foam type (e.g., foam density and foam microstructure), the results reported by Yu et al.[94] and Linul et al.[96] highlight different answers.

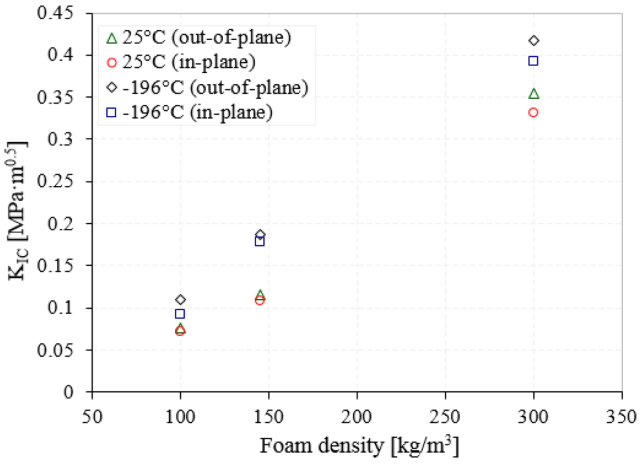

FIGURE 23 In-plane and out-of-plane K_{IC} results according to operating temperature[96] [Colour figure can be viewed at wileyonlinelibrary.com]

Based on their data, Linul et al.[96] proposed a linear correlation for estimation of K_{IC} at cryogenic temperature ($K_{IC,-196}$) according to room temperature values, in the form of Equation 24:

$$K_{IC,-196} = 1.0728\ K_{IC,+25} + 0.0405 \quad \text{with} R^2 = 0.9825. \tag{24}$$

4.6 | Size effect

It was proven that the brittle materials exhibit a pronounced size effect.[97] The size effect on fracture of polymeric foams (PVC, density 100 kg/m^3) was first investigated by Bazant et al.[98] They used notched tensile specimens with the same thickness (25.40 mm) but having three different widths (6.35, 43.94 and 304.80 mm) and a constant length to width ratio (5:2). According to their results, a strong size effect in closed cell PVC foams occurs. The foams behaviour agrees well the size effect law of Bazant,[99] based on asymptotic matching, which represents a smooth transition between asymptotic case corresponding to LEFM and no size effect.

Linul et al.[100] and Marsavina et al.[75] studied the size effect on PUR foams by using SENB specimens. They investigated the dependence of the nominal stress $\sigma_N = (3P_{max}S)/(2BW^2)$ as a function of the characteristic size of the specimen W, in this case, the specimen width. The specimens were cut from plates and had the same thickness B of approximately 53 mm for PUR foams of 100- and 145-kg/m^3 density, respectively 25 mm for 300 kg/m^3. Similar geometrical specimens with different width W = 5.5 (XS), 10.0 (S), 25.4 (M), 53.7 (L) and 224.5 (XL) mm and length-to-width ratio 4 were tested in TPB. Typical load–displacement curves obtained for testing the different size specimens are shown in Figure 24 for 100-kg/m^3 foam density. The results are plotted in Figure 25; in logarithmic coordinates Log (σ_N) versus Log (W), the markers represent the average experimental results and the black line the asymptotic Equation 25. If the failure of the foam obeys LEFM, the logarithmic size effect plot would have to be a straight line with the slope −1/2, shown dotted in Figure 25. A ductile behaviour following the strength criteria (SC) with no size effect would be a horizontal line $\sigma_N = \sigma_f$, with σ_f fracture or yield stress of the foam. The obtained experimental results are asymptotic to these approaches having the form[97,99]:

$$\sigma_N = \frac{\sigma_{N0}}{\sqrt{1 + \frac{W}{W_0}}} \tag{25}$$

where σ_{N0} and W_0 are fitting parameters.

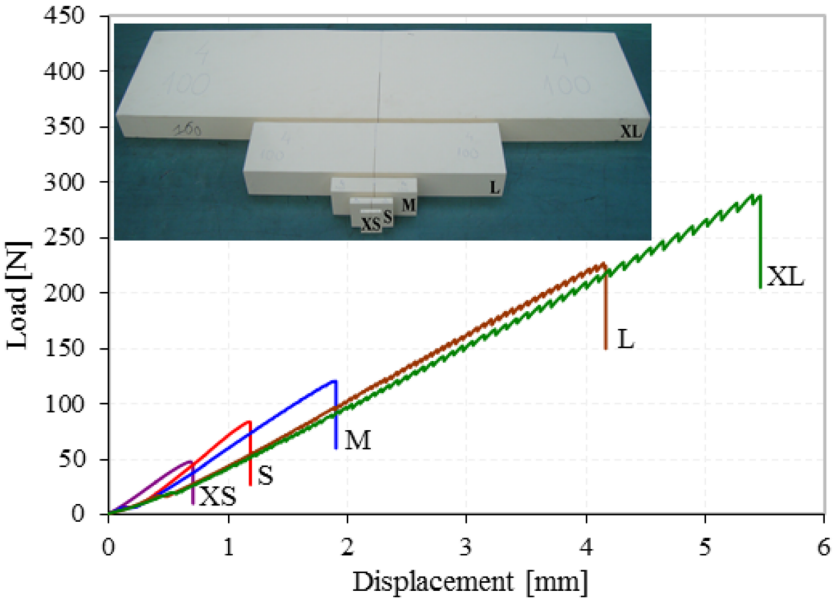

FIGURE 24 Typical load–displacement curves for different specimen sizes of foam with 100-kg/m^3 density [Colour figure can be viewed at wileyonlinelibrary.com]

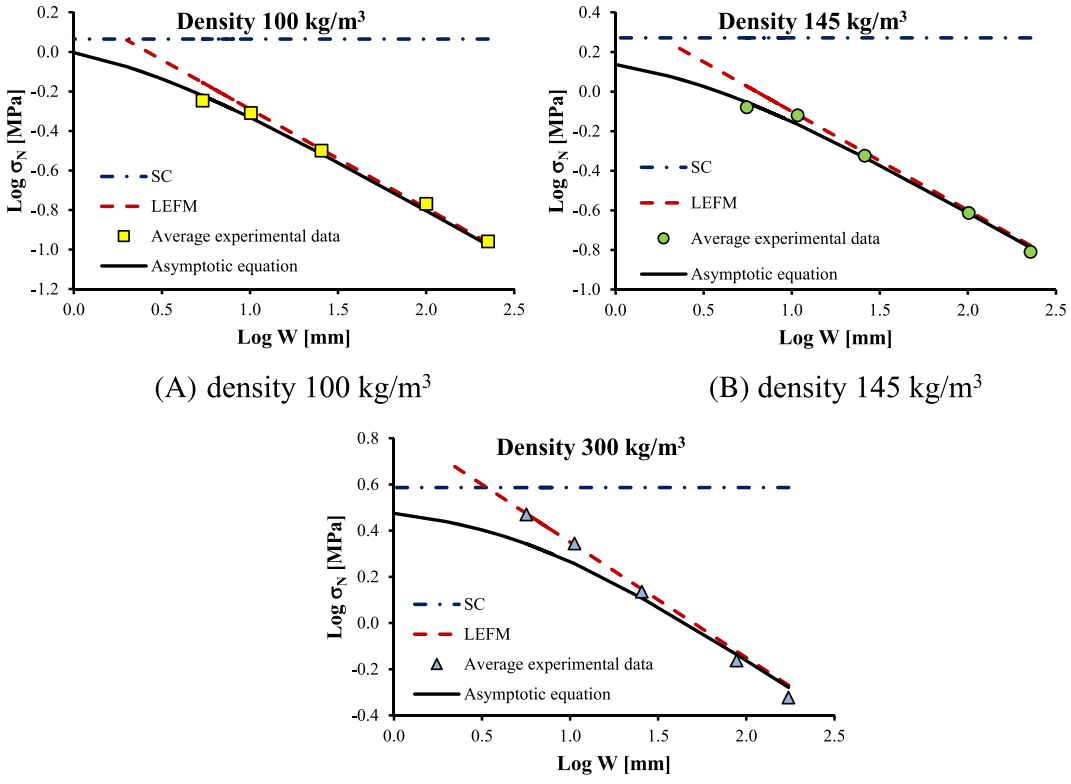

(A) density 100 kg/m^3 (B) density 145 kg/m^3

(C) density 300 kg/m^3

FIGURE 25 The size effect of three different PUR foam densities with single-edge notched bending specimens subjected to three-point bending [Colour figure can be viewed at wileyonlinelibrary.com]

It can be seen that for all specimen sizes, the LEFM fits better the experimental results. The fitting parameters from Equation 25 σ_{N0} and W_0 increase with foam density and are shown in Table 4. These results show that the design of PUR foam structures based on strength or plasticity criteria is generally valid only for small structural parts, whereas for large components, the LEFM concepts should be used.

Touliatou and Wheel[101] observed also a prominent size effect on brittle materials with low and medium

TABLE 4 Size effect results

Density (kg/m^3)	Cell size (mm)	σ_f (MPa)	σ_{N0} (MPa)	W_0 (mm)
100	0.104	1.16	1.275	1.542
145	0.084	1.87	1.651	2.232
300	0.068	3.86	3.297	4.545

porosity. As the specimen size increases, the material becomes less tough, until it converges to a specific value. As expected, a weakening effect is also exhibited with increasing porosity.

5 | MIXED-MODE FRACTURE TOUGHNESS

Structures containing foams, such as sandwich structures, are often subjected to mixed-mode loading. However, only few fracture toughness results are published for mixed-mode loading of plastic foams.

5.1 | Phenomenological models

The interpretation of in-plane mixed-mode (opening and in-plane shear) fracture results were based on the well-known phenomenological fracture criteria, which implies a relationship between stress intensity factors (K_I and K_{II}) and the fracture toughness (K_{IC}): $f(K_I, K_{II}, K_{IC}) = 0$, respectively the angle of crack initiation θ_c.

Among these criteria, the *maximum circumferential tensile stress* (MTS) of Erdogan and Sih,[102] *minimum strain energy density* (SED) of Sih,[103] *maximum energy release rate criterion* (Gmax) of Hussain et al.[104] and *equivalent stress intensity factor* (ESIF) of Richard[105,106] are often employed. Hallsträm and Grenestedt[107] investigated mixed-mode fracture of cracks and wedge-shaped notches in expanded PVC foams. Different types of specimens made of Divinycell H100 were investigated and the non-singular *T*-stress was considered in the formulation of fracture criteria. It was concluded that for predominantly mode II, the use of *T*-stress improved the facture predictions. Noury et al.[108] tested three different PVC foams densities (90, 130 and 200 kg/m^3) using a SEC specimen with Arcan grips in order to produce mixed-mode conditions. Figure 26 presents their results together with fracture envelopes based on the mentioned criteria. It could be concluded that for rigid PVC foams the Richard's ESIF criterion is most reliable to predict mixed-mode fracture. This could be also explained by the fact that it takes into account the ratio between mode I and mode II fracture toughness $\alpha = K_{IC}/K_{IIC}$.

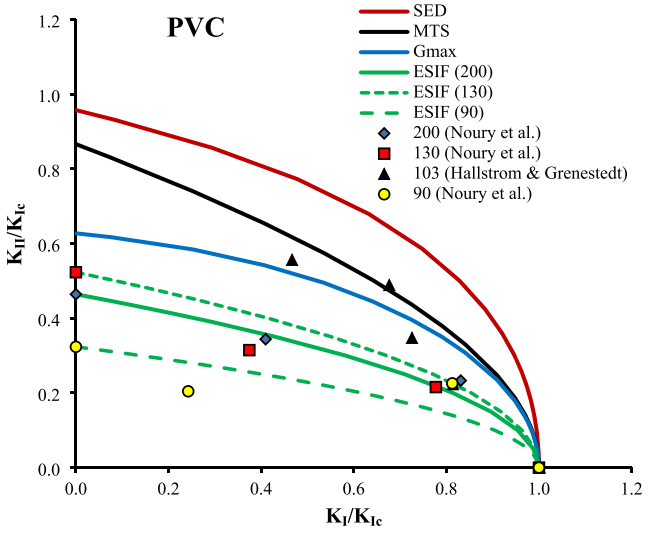

FIGURE 26 Mixed-mode fracture results for PVC rigid foams, adapted from Hallsträm and Grenestedt[107] and Noury et al.[108] [Colour figure can be viewed at wileyonlinelibrary.com]

Burman[69] experimentally determined the mode I (on CT specimens) and mode II (on end notched flexure specimens) fracture toughness of PVC foam Divinicell H100 (density 100 kg/m^3) and WF51 (density 52 kg/m^3) resulting: $K_{IC,H100} = K_{IIC,H100} = 0.21$ MPa m$^{0.5}$, respectively $K_{IC,WF51} = 0.08$ MPa m$^{0.5}$, $K_{IIC,WF51} = 0.13$ MPa m$^{0.5}$.

Marsavina et al.[75] using ASCB specimens, Linul et al.[109,110] on SEC specimens and Apostol et al.[111] on SENB specimens loaded on FPB presented extensive studies on the assessment of mixed-mode fracture criteria for PUR foams. The experimental results and fracture envelopes are summarized in Figure 27A–C. Figure 27 presents the mean values of the ratio between K_{II}/K_{IC} versus K_I/K_{IC}, together with the fracture curves predicted by the phenomenological criteria. For foams with densities 100 and 145 kg/m^3, the effect of cell orientation was also investigated.

It can be observed that for low-density foams (100- and 145-kg/m^3 densities), the experimental results fall between the G_{max} and ESIF criteria for all types of specimens, whereas for the foam with 300 kg/m^3, the experimental data are more scattered and close to SED and ESIF criteria. Based on these results, it could be concluded that also for rigid PUR foams, Richard's ESIF criterion is most reliable to predict mixed-mode fracture. This could be explained by the fact that Richard[105] criteria trigger the fracture data with $\alpha = K_{IC}/K_{IIC}$. The mixed-mode fracture is slightly different on the two considered cell orientations (rise and flow directions) (Figure 27A,B).

An important parameter for mixed-mode loading is the ratio between mode II and mode I fracture toughness

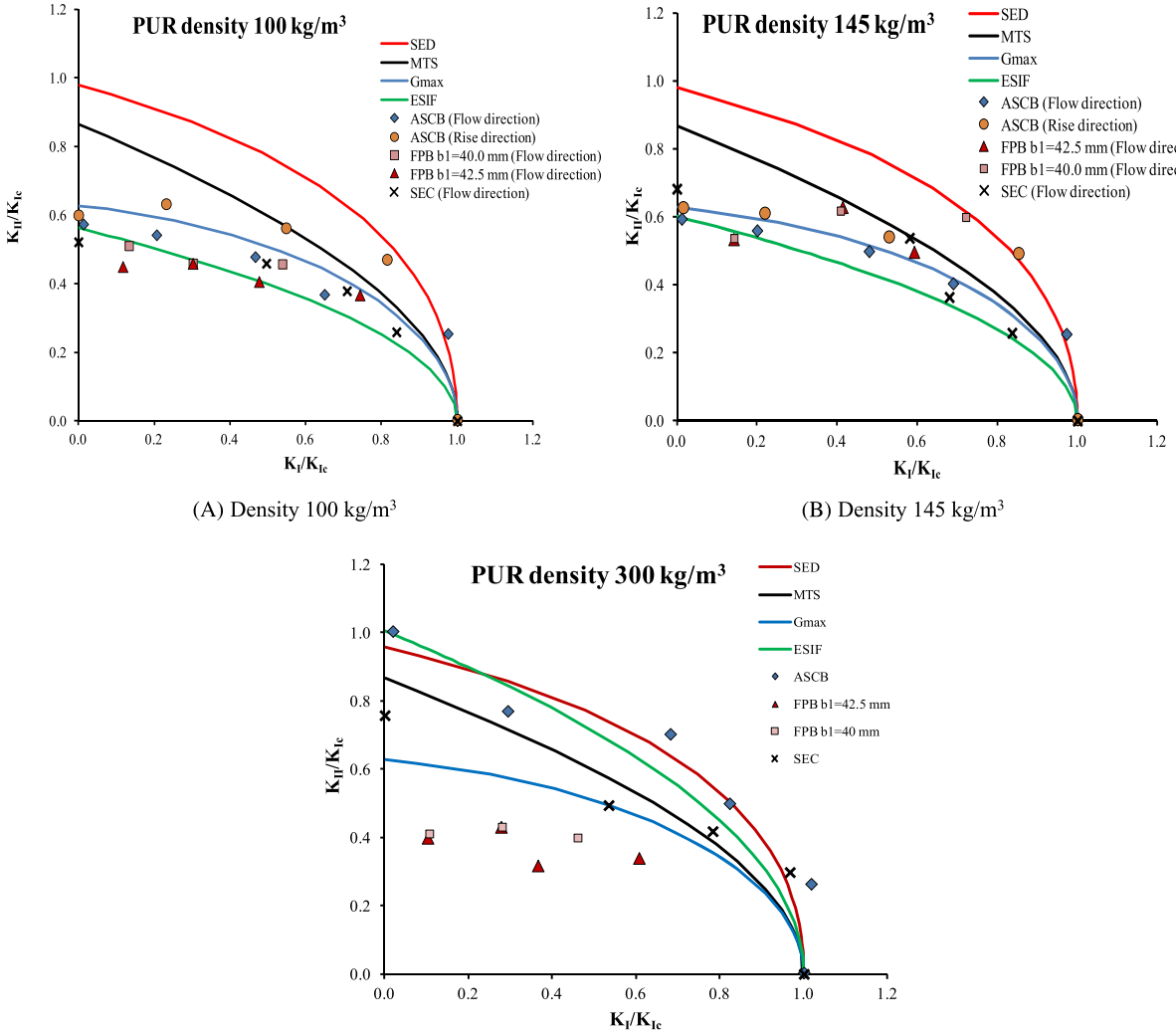

(A) Density 100 kg/m^3

(B) Density 145 kg/m^3

(C) Density 300 kg/m^3

FIGURE 27 Mixed-mode fracture results for rigid PUR foams of different densities, based on Marsavina et al.[75] on asymmetric semicircular bend (ASCB) specimens, Linul et al.[109,110] on single-edge crack (SEC) specimens and Apostol et al.[111] on single-edge notched bending specimens loaded in four-point bending (FPB) [Colour figure can be viewed at wileyonlinelibrary.com]

K_{IIC}/K_{IC}. Experimental results performed on ASCB, SENB loaded in TPB and FPB and SEC highlighted that ratio K_{IIC}/K_{IC} is between 0.47 and 1 for PUR foams increasing with density, which is in agreement with results of Noury et al.[108] for PVC foam with a ratio in the range 0.36 to 0.6 (Figure 28).

Figure 29 presents the mean values of the crack initiation angle θ_c measured on ASCB and SEC PUR foam specimens versus applied mixed-mode loading $Me = (1/\pi)\tan^{-1}(K_{II}/K_I)$, side by side with the predicted crack initiation angles predicted by fracture criteria. It could be observed that for predominantly mode I loadings $Me < 45^\circ$, the measured values of the crack initiation angle are in good agreement with the predicted ones. For predominantly mode II loading ($Me > 45^\circ$), the experimental crack propagation angles differ to the predicted values, the closest to the phenomenological predictions were obtained for SEC specimens.

Simulation of crack initiation and propagation in PUR foams was investigated numerically using extended FE method by Marsavina et al.[112,113] for mixed-mode cracks and by Apostol et al.[114] for mode II cracks. In both studies, the simulated crack propagation paths are in good agreement with the observed experimental paths (Figure 30).

As an important conclusion to be drawn is that the phenomenological fracture criteria, developed for solid materials, could be successfully extended to predict the fracture limit and the crack initiation angle for foam materials.

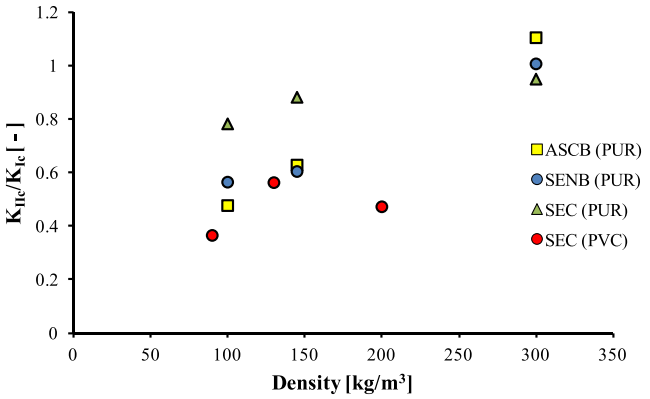

FIGURE 28 The ration K_{IIC}/K_{IC} versus density for PUR foams (asymmetric semicircular bend [ASCB] specimens from Marsavina et al.,[75] single-edge notched bending [SENB] in three-point bending from Marsavina et al.,[68] SENB in four-point bending from Apostol et al.,[73,74] single-edge crack (SEC) from Linul and Marsavina[110] and PVC foam from Noury et al.[108]) [Colour figure can be viewed at wileyonlinelibrary.com]

5.2 | Empirical models

Empirical relationships between ratios K_{II}/K_{IIC} and K_I/K_{IC} were proposed in the literature to assess mixed-mode fracture.[115,116] A general relation can be expressed in the form:

$$\left(\frac{K_I}{K_{IC}}\right)^p + \left(\frac{K_{II}}{K_{IIC}}\right)^q = 1 \tag{26}$$

where p and q are fitting parameters. The parameters can be equal $p = q = \alpha$ according to Lim et al.,[115] or $p \neq q$ ($p = 1$ and $q = 2$).[116] For exemplification empirical prediction, for $\alpha = 1.5$, 1.75 and 2 respectively $p = 1$ and $q = 2$, are plotted with the experimental fracture toughness results obtained on PUR specimens of three different densities and two types of specimens (ASCB and SEC) and indicate a good correlation for all foam densities (Figure 31).

In a recent study, Aliha et al.[77] presented some results on mode III and mixed-mode (I + III) fracture toughness of PUR foams. They employed edge-notched disc bend (ENDB) specimens, for three foam densities (100, 145 and 300 kg/m^3). The specimen dimensions were $R = 75$ mm, $B = 30$ mm, $a = 15$ mm and $S = 37$ mm (Figure 32). The experimental data expressed in the fracture plane K_{III}/K_{IC} versus K_I/K_{IC} show good agreement with the maximum tangential strain energy density (MTSED) criterion (Figure 33).

They also investigate the crack initiation angle and propagation paths for mixed-mode I and III (Figure 34).[117]

The experimental studies for determining K_{IC} were performed using wide range of specimens and different solid materials (PUR, PVC and PIR). The obtained results vary between 0.01 and 0.63 MPa m$^{0.5}$. The effect of loading speed, foam anisotropy, testing temperature and the size effect was also experimentally investigated. Fewer studies investigated the fracture criteria under mixed-mode loading (I + II and I + III) and the crack initiation angle, using phenomenological or empirical models.

6 | DYNAMIC FRACTURE TOUGHNESS

There are only few results reported in the literature regarding the dynamic fracture toughness of plastic foams. Kabir et al.[67] investigated the mode I dynamic fracture toughness of PVC foam with 260-kg/m^3 density and obtained a maximum value of 2.74 MPa m$^{0.5}$, which is approximately 3.75 times higher than the static fracture toughness of the same foam.

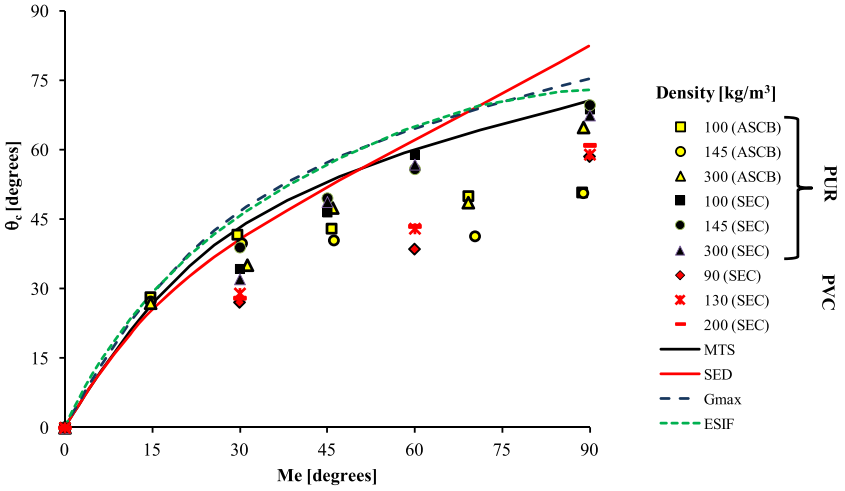

FIGURE 29 Comparison of predicted and experimental crack initiation angles[75,108,109] [Colour figure can be viewed at wileyonlinelibrary.com]

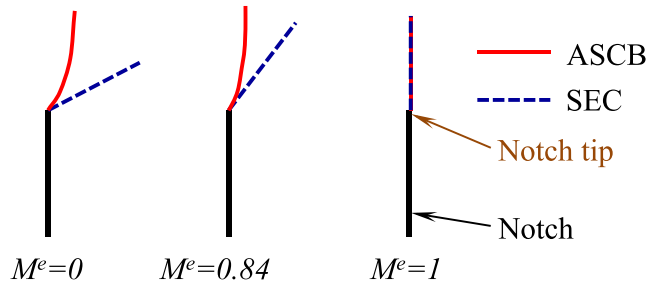

FIGURE 30 Crack propagation paths for mixed-mode I/II fracture (asymmetric semicircular bend [ASCB] and single-edge crack [SEC] specimens)[111,112] [Colour figure can be viewed at wileyonlinelibrary.com]

Mills and Kang[118] used CT specimens (20 mm thick and 50 mm × 50 mm size) made from polystyrene (PS) and a special designed falling mass equipment with 1.85-m/s velocity in order to determine the dynamic fracture toughness. The investigated PS is used for helmet and box lid having the density in the range 20–85 kg/m^3, and some tests were carried on specimens immersed in water for 24 h. They proposed a correlation between dynamic fracture toughness and relative density in the form $K_{ID} = 0.955\,\rho^{1.119}$.

Marsavina and Sadowski[119] investigated the effect of an impregnation layer on dynamic fracture toughness of polyurethane rigid foams. They investigated closed cell rigid PUR foam with 200-kg/m^3 density, manufactured and supplied in the form of flat panels of 12-mm thickness. The foam faces were impregnated with epoxy (layer of 170 μm) and polyester (layer of 100 μm) resin. SENB specimens (12 mm × 12 mm × 60 mm) were adopted with a notch of 1.5 mm (cut with a razor blade), a span of 40 mm was used for the test and the impact load was applied using an instrumented impact hammer. The

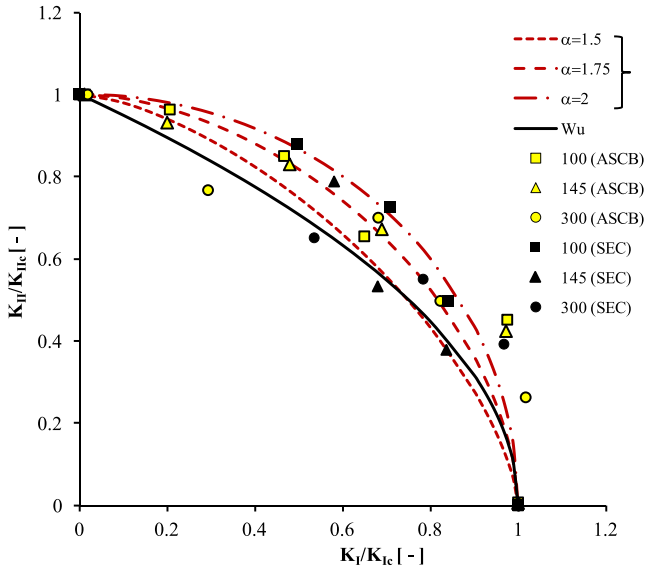

FIGURE 31 Empirical fracture models together with experimental data for PUR foam using asymmetric semicircular bend (ASCB)[75] and single-edge crack (SEC) specimens[109,110] [Colour figure can be viewed at wileyonlinelibrary.com]

mean values of the dynamic fracture toughness for unimpregnated specimens was 0.202 MPa m$^{0.5}$ and approximately 26% higher for the impregnated specimens.

Marsavina et al.[120] presented a correlation between static and dynamic fracture toughness for PUR foams in the density range 40–160 kg/m^3. Single-edge notched specimens (thickness B = 13 mm, width W = 25 mm) under TPB (span S = 100 mm) were used for both static and dynamic tests. The impact tests were carried out using a KB Pruftechnik instrumented pendulum. Linul et al.[96] presented the dynamic fracture toughness for PUR foams of three densities (100, 145 and

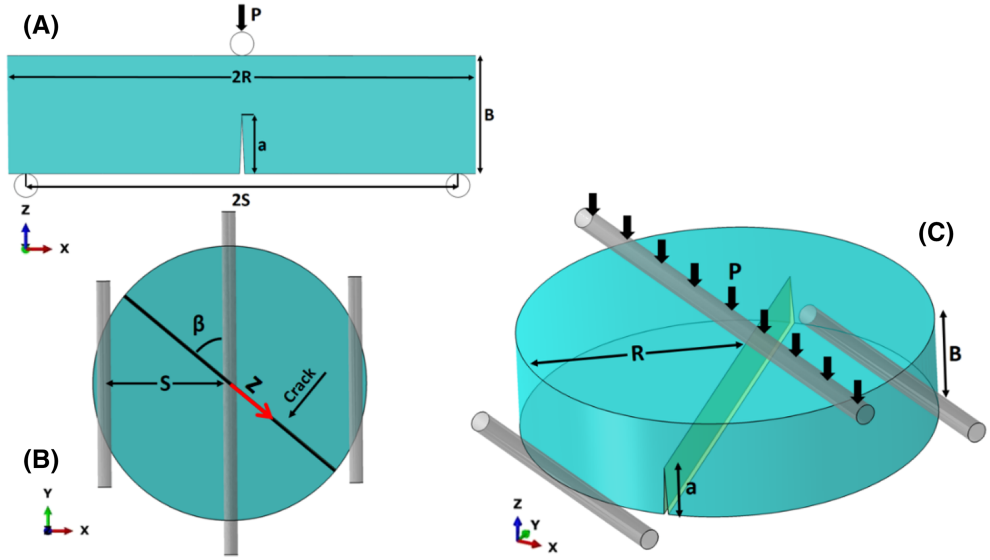

FIGURE 32 Loading configurations of the edge notched disc bend specimen[77] [Colour figure can be viewed at wileyonlinelibrary.com]

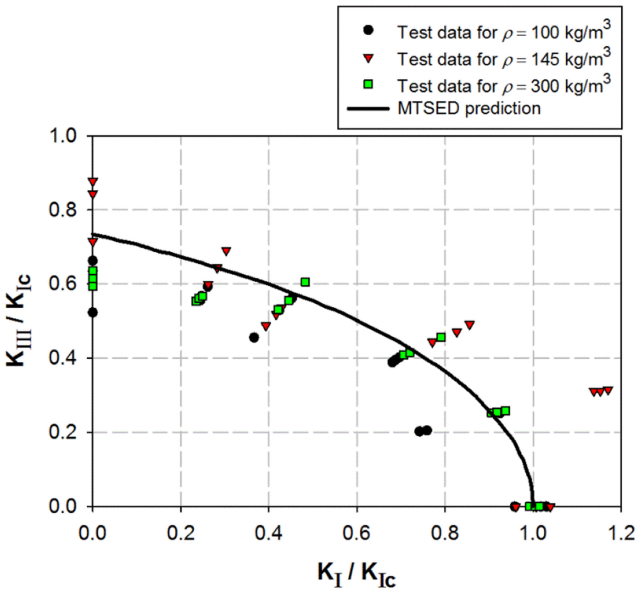

FIGURE 33 Mixed-mode (I + III) fracture results for rigid PUR foams of different densities together with maximum tangential strain energy density (MTSED) criterion[77] [Colour figure can be viewed at wileyonlinelibrary.com]

300 kg/m^3) determined following the same methodology of Marsavina et al.[120]

For each density, the dynamic fracture toughness values are higher than the static fracture toughness values and a linear correlation between K_{IC} and K_{ID} was proposed (Figure 35), valid in the considered density range, which could be useful for estimation of dynamic fracture toughness if static fracture toughness values are available.

7 | IMPROVING FRACTURE TOUGHNESS BY REINFORCING THE FOAMS

Different materials for reinforcement (Rajak et al.[121]) are used to improve the physical and mechanical properties of polymeric foams starting from glass fibre (Serban et al.[122]) or aluminium microfibres (Linul et al.[123,124]) to potato protein (Członka et al.[125]).

Cotgreave and Shortall[126] presented one of the first investigation to improve the fracture toughness of rigid closed cell PUR foam, by reinforcing with CGFs. The incorporation of GFs provides an extension of the natural toughening mechanism, arising from microstructural features that provide for multiple arrests and diversions to occur along the path of a propagating crack. The fibres serve to increase the elastic modulus of the foam and this result in higher fracture toughness values even though the fracture surface energy shows no increase. Some

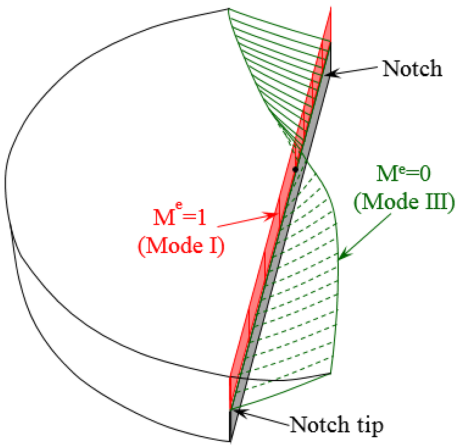

FIGURE 34 Crack propagation paths for mixed-mode I/III fracture (edge-notched disc bend specimens)[117] [Colour figure can be viewed at wileyonlinelibrary.com]

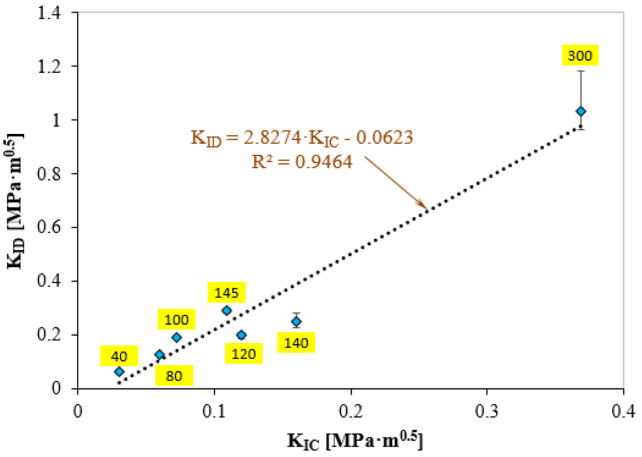

FIGURE 35 Linear correlation between dynamic and static fracture toughness, adapted from Marsavina et al.[120] and Linul et al.[96] [Colour figure can be viewed at wileyonlinelibrary.com]

contribution to the fracture toughness may be attributed to the work required to the extract the unique "pull-out" fragments, Figure 36. The fracture toughness of the composite is directly proportional to the fibre content.

Chen and Gibson[127] investigated foam materials by mixing up to 50% volume fraction of 50 μm diameter hollow glass microspheres (3 M Industrial Specialties Division) with epoxy resin. SENB specimens were tested for fracture toughness determination and the performance indices: $(K_{IC}/\rho, K_{IC})^{2/3}/\rho$ and $(K_{IC})^{1/2}/\rho$ were determined. The fracture toughness decreases from the pure epoxy resin to foam material with 45% volume fraction of spheres. However, the performance indices increased with the increase of hollow sphere volume fractions.

The effect of the fibre content and fibre length on tensile, fracture and thermal properties of syntactic foam

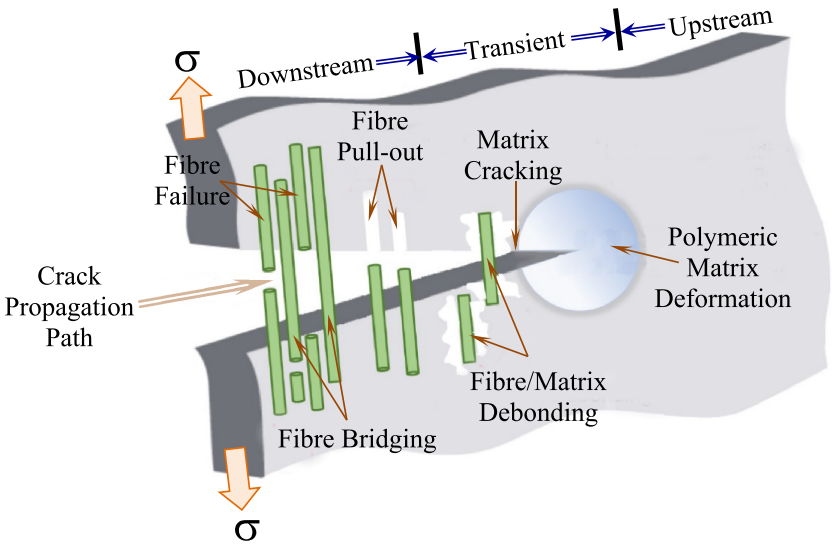

FIGURE 36 Typical failure modes in reinforced polymeric foams and process zone near the crack tip [Colour figure can be viewed at wileyonlinelibrary.com]

was investigated by Wouterson et al.[128] The syntactic foam was produced by mechanical dispersion of 30 vol.% hollow phenolic microspheres (Phenoset BJO-093) as filler in epoxy resin. Short carbon fibre (CF) having 7-μm diameter were used for reinforcement in weight fraction of 1, 2 and 3 wt%. The results showed that a hybrid structure demonstrates a significant increase in the ultimate tensile strength and Young's modulus with increasing fibre volume fraction. Interestingly, the fracture toughness K_{IC} and energy release rate G_{IC} increased by 95% and 90%, respectively, upon introduction of 3 wt% short CFs in syntactic foam, indicating the toughening potential for short CFs in syntactic foam systems. SEM and OM studies identified the presence of several toughening mechanisms. An estimate of the contribution from each toughening mechanism by composite theory and fractography revealed that the specific energy required to create new surfaces was enhanced by the presence of fibres and was the main contributor to the toughness of the short fibre reinforced syntactic foam. However, the variation in fibre length between 3 and 10 mm does not affect the tensile and fracture properties significantly.

Maharsia and Jerro[129] investigated nanoclay hybrid syntactic foams. Four types of hollow glass particles (3 M Corporation) with different densities were used for fabrication. The foams were fabricated with a constant (35%) volume fraction of resin and 65% filler particles. Eight types of nanoclay hybrid foams are made by combining two volume fractions of nanoclay particles (2% and 5%, respectively) with each microballoon type. Results from tensile testing show that strength has increased in all hybrid foams because of the presence of nanoclay particles. Addition of 5% nanoclay results in strength enhancement of between 6% and 22%. Damage tolerance has also increased because of increase in plasticity of matrix because of nanoclay clusters and surfactants on nanoclay particles. It is seen that between 33% and 58% increase in toughness of high-density foams is obtained with the addition of 5% nanoclay particles.

Different microstructures were manufactured using three different types of microspheres, namely, 3 M Scotchlite, TM K15 and K46 glass bubbles and Phenoset BJO-093 hollow phenolic microspheres, and by modifying the volume fractions of microspheres from 0% to 50% volume fraction.[130] The fracture toughness tests were performed using SENB specimens loaded in TPB under quasi-static loading. The fracture toughness and the specific fracture toughness/performance index K_{IC}/ρ increase up to 30 vol% for all types of microspheres and then decrease beyond 30 vol% of filler content. The change in behaviour was attributed to a change in the dominant toughening mechanisms from filler stiffening, crack front bowing to excessive debonding of microspheres in reduced matrix volume.

Wouterson et al.[131] investigated the effect of nanoclay content on tensile and fracture properties of syntactic foam. Results showed that the tensile strength decreased slightly with increasing nanoclay content. The Young's modulus showed an increase of 17% with the addition of 2-wt% clay. Interestingly, the fracture properties reached a maximum for samples containing 1 wt% of nanoclay. SEM and OM studies were performed to identify the toughening mechanisms in nanoclay-reinforced syntactic foam. A comparison of the tensile and fracture results obtained for nanoreinforced syntactic foam against short-fibre reinforced syntactic foam revealed the superiority of micro-reinforcements over nano-reinforcements in improving the tensile properties. Both short microfibres and nanoclay were able to give rise to substantial increase in toughness in polymer syntactic foam.

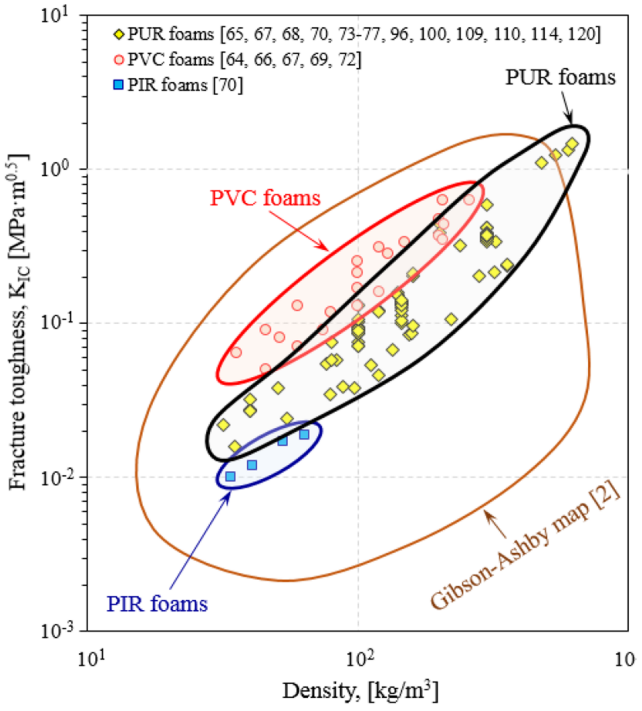

FIGURE 37 Fracture toughness-density chart for families of polymeric foams [Colour figure can be viewed at wileyonlinelibrary.com]

Stewart et al.[132] developed polyurethane foam reinforced with SiC nanoparticles for core in sandwich composites. The functionalization of SiC nanoparticles was performed using a silane-coupling agent to enhance bonding between PU and SiC particles. The SENB specimens loaded in TPB show that the reinforcement of SiC nanoparticles by 1.0 wt% improved the compressive and flexural properties by 50%–70% range. While with the functionalization of SiC particles, an improvement with 200% was observed. The fracture toughness is reduced by SiC reinforcement.

Gómez-Monterde et al.[133] presented an analysis on morphology, mechanical properties and fracture behaviour of solid and foamed plates made of GF-reinforced Polypropylene. The determined fracture parameters were crack tip opening displacement (CTOD) at low strain rate and the fracture toughness (K_{IC}) at impact loading. Foamed specimens presented higher values of CTOD than the solid ones and higher as the foaming ratio increases, because of cells acting as crack arrestors by blunting the crack tip. On the contrary, the fracture toughness K_{IC} decreased with decreasing the apparent density. Because of stress concentration on cell walls, lower density and energy absorption capability, the fracture toughness decreases with approximately 20% for 10% foaming ratio, respectively with 40% for the foaming ratio of 20%. Anisotropy due to fibre orientation was also observed. Fibres were aligned in the filling direction in the surface layers, while they were oriented in the transverse direction in the core. Different properties were obtained with fibres orientation.

Idowu et al.[134] presented a review on three-dimensional graphene foam reinforced polymer matrix composites. Graphene as a filler is being considered to address challenging issues of graphene dispersion and restacking in composite materials because of its three-dimensional interconnected hierarchical structure and its physical–chemical attributes. The stress–strain curve for tensile tests of the graphene foam reinforced polymer matrix composites reveals that the fracture occurs at 45° plane, Nieto et al..[135] The graphene foam reinforced polymer matrix composites allows crack deflection, resulting in enhancement of fracture toughness of the graphene foam-based composite. The same conclusions were observed by Jia et al.[136]

An interesting study on self-healing microvascular polymeric foam for improving the toughness of brittle polyisocyanurate (PIR) foam is presented by Patrick et al.[137] They investigated the healing of brittle PIR foam (Trymer 3000, density 50 kg/m^3) under mode I loading using SENB specimen. The fracture toughness of PIR foam was 0.02 MPa m$^{0.5}$. The healing consists in prefilling of the microvascular channel with the desired healing component and subsequently connecting the open tubing at a wye junction, resulting in a closed system. The expansive nature of the PUR foam reaction provided fast healing, with over 75% recovery in both stiffness and fracture toughness in 1 h at room temperature. The fracture toughness of healed components was 0.018 for horizontal channels, respectively 0.019 MPa·m$^{0.5}$ for vertical channels.

Foam reinforcement was adopted to increase the mechanical and fracture properties of polymeric foams. Glass fibres, CFs, aluminium microfibers, nanoclay particles, SiC nanoparticles and graphene were used to reinforce the foams.

8 | CONCLUDING REMARKS

Efforts in evaluation of the fracture toughness of polymeric foams are clustered around few themes and methodologies. Researches focused on the macroscopic behaviour involving experimental investigations, respectively on the micromechanical aspects of fracture, which are based on analytical and computational analysis.

Analytical and numerical micromechanical models are reviewed and they can successfully be applied to predict the fracture toughness of plastic foams.

However, the fracture toughness values obtained via micromechanical analysis should be experimentally validated.

The analytical micromechanical models estimate the fracture toughness of the foams based on mechanical properties of solid material from cell struts and faces (tensile strength), relative density and some fitting parameters based on cell topology (cell length, strut thickness). There are available models to predict fracture toughness for all fracture modes K_{IC}, K_{IIC} and K_{IIIC}.

The numerical FE micromechanical models allow the investigation of more complex 2D and 3D cellular structures (beams, 2D and 3D solids) with different struts cross sections. The cracks are modelled like broken struts/cells. Usually, the prediction of fracture toughness is based on the applied load, which produce the fracture of the first unbroken strut, and on the LEFM solutions.

At the end of this review, we can conclude that LEFM could be applied for rigid plastic foams. In order to use the LEFM in designing such structures, the fracture toughness of materials should be known, particularly for large structures, if tensile and bending loads are present. Experimental procedure for fracture toughness determination is presented, together with a comprehensive set of experimental results for the fracture toughness.

The fracture toughness of rigid polymeric foams is expressed mainly by K_{IC} and G_{IC}; for flexible foams, the essential work of fracture could be also used.[138]

The experimental results indicate that the fracture toughness does not depend on the specimen shape being a material constant. The density plays the major role on the fracture toughness; this can be observed also in a fracture toughness–density diagram (Figure 37), followed by the solid material contained in the struts and faces.

The foam anisotropy was identified as having different fracture toughness values in the flow and rise direction. This effect is related to the shape of the cells in the two directions and could be quantified considering the cell structure dimensions (strut thickness and cell length). An increase of the fracture toughness was observed at cryogenic temperatures −196°C comparing with those at room temperature.

The investigations on the size effect show that all results are closer to LEFM behaviour. This should be taken into account when design of such structures, because the strength or plasticity criteria are valid only for small structural parts. In the case of large components, the size effect and LEFM should be considered.

The classical fracture criteria, developed for brittle isotropic materials, were applied with success for mixed-mode loading of polymeric foams. The best predictions were obtained for *equivalent stress intensity factor* and for the *maximum energy release rate* criteria for mixed modes I and II, respectively the *maximum tangential strain energy density* criterion for mixed modes I and III.

The dynamic fracture toughness values are higher than the static ones with approximately 2.8 times for all densities between 40 and 300 kg/m^3.

The fracture toughness could be increased by reinforcing the foam with different particles and/or fibres.

ACKNOWLEDGEMENT

This paper was partially funded by the Romanian Ministry of Research and Innovation through projects 10PFE/16.10.2018, PERFORM-TECH-UPT and PN-III-P1-1.2-PCCDI-2017-0391 and by the European Union's Horizon 2020 research and innovation programme under grant agreement no. 857124.

REFERENCES

1. Ashby MF. Cellular solids scaling of proprieties. In: Scheffler M, Colombo P, eds. *Cellular Ceramics: Structure, Manufacturing, Properties and Applications*. Wiley-VCH Verlag Gmbh & Co; 2005:3-16.
2. Gibson LJ, Ashby MF. *Cellular Solids, Structure and Properties*. Second ed. Cambridge University Press; 1997.
3. Mills NJ. *Polymer Foams Handbook*. Butterworth-Heinemann; 2007.
4. Marsavina L. Fracture mechanics of foams. In: Altenbach H, Ochsner A, eds. *Cellular and Porous Materials in Structures and Processes*. Springer; 2010:1-46.
5. Marsavina L, Constantinescu DM. Failure and damage in cellular materials. In: Altenbach H, Sadowski T, eds. *Failure and Damage Analysis of Advanced Materials*. Springer; 2015: 119-190.
6. Grenestedt JL. Effective elastic behavior of some models for perfect cellular solids. *Intern J So Struc*. 1999;36(10):1471-1501.
7. Onck PR, Andrews EW, Gibson LJ. Size effects in ductile cellular solids. Part I: modelling. *Intern J Mecha Sci*. 2001;43: 681-699.
8. Saint-Michel F, Chazeau L, Cavaille J-Y, Chabert E. Mechanical properties of high density polyurethane foams: I. Effect of the density. *Comp Sci and Techn*. 2006;66(15):2700-2708.
9. Christensen RM. A comparison of open cell and closed cell properties for low-density materials. *J Mech of Mate and Struct*. 2007;2(7):1299-1307.
10. Avalle M, Belingardi G, Montanini R. Characterization of polymeric structural foams under compressive impact loading by means of energy-absorption diagram. *Int J Imp Eng*. 2001; 25(5):455-472.
11. Avalle M, Belingardi G, Ibba A. Mechanical models of cellular solids: parameters identification from experimental tests. *Int J of Impact Engineering*. 2007;34(1):3-27.
12. Lagzdins A, Zilaucs A, Beverte I, Andersons J, Cabulis U. A refined strut model for describing the elastic properties of highly porous cellular polymers reinforced with short fibers. *Mech Comp Mate*. 2017;53(3):321-334.
13. Mills NJ, Zhu H. The high strain compression of closed cell polymer foams. *J Mech Phys Solids*. 1999;47(3):669-695.

14. Huang JS, Chow CI. Survival probability for brittle isotropic foams under multiaxial loading. *J Mater Sci*. 2000;35(15):3881-3887.
15. Gupta N, Ricci W. Comparison of compressive properties of layered syntactic foams having gradient in microballoon volume fraction and wall thickness. *Mater Sci Eng A*. 2006;427(1-2):331-342.
16. Alonso IQ, Fleck NA. Damage tolerance of an elastic-brittle diamond-celled honeycomb. *Scr Mater*. 2007;56:693-696.
17. Romijn NER, Fleck NA. The fracture toughness of planar lattices: imperfection sensitivity. *J Mech Phys Solids*. 2007;55(12):2538-2564.
18. Ren XJ, Silberschmidt VV. Numerical modelling of low-density cellular materials. *Comput Mater Sci*. 2008;43:65-74.
19. Pinto H, Amini A, Pena A, Moraga P, Valenzuela M. Fatigue and damage accumulation in open cell aluminium foams. *Fatigue Fract Eng Mater Struct*. 2018;41(2):483-493.
20. Kucherov L, Ryvkin M. Flaw nucleation in a brittle open-cell Kelvin foam. *Int J Fract*. 2012;175(1):79-86.
21. Kucherov L, Ryvkin M. Fracture toughness of open-cell Kelvin foam. *Intern J So Struc*. 2014;51(2):440-448.
22. Fleck NA, Desphande VS, Ashby MF. Micro-architectured materials: past, present and future. *Proc R Soc A*. 2010;466(2121):2495-2516.
23. Ashby MF. The mechanical properties of cellular solids. *Metall Trans A*. 1983;14A:1755-1768.
24. Maiti SK, Ashby MF, Gibson LJ. Fracture toughness of cellular solids. *Scripta Metallur*. 1984;18(3):213-217.
25. Fowlkes CW. Fracture toughness tests of a rigid polyurethane foam. *Intern J Frac*. 1974;10(1):99-108.
26. Mclntyre A, Anderton GE. Fracture properties of a rigid polyurethane foam over a range of densities. *Polymer*. 1979;20(2):247-253.
27. Brezny R, Green DJ. Fracture behavior of open-cell ceramics. *J Amer Ceramic Society*. 1989;72(7):1145-1152.
28. Huang JS, Gibson LJ. Fracture toughness of brittle honeycombs. *Acta Metallurgica et Materialia*. 1991;39(7):1617-1626.
29. Huang JS, Gibson LJ. Fracture toughness of brittle foams. *Acta Metallurgica et Materialia*. 1991;39(7):1627-1636.
30. Green DJ. Fabrication and mechanical properties of lightweight ceramics produced by sintering of hollow spheres. *J. Ame Cer Soc*. 1985;48:403-409.
31. Choi S, Sankar BV. A micromechanical method to predict the fracture toughness of cellular materials. *Intern J So Struc*. 2005;42(5-6):1797-1817.
32. Choi JB, Lakes RS. Fracture toughness of re-entrant foam materials with a negative Poisson's ratio: experiment and analysis. *Int J Fracture*. 1996;80(1):73-83.
33. Fan HL, Fang DN. Enhancement of mechanical properties of hollow-strut foams: analysis. *Mate and De*. 2009;30(5):1659-1666.
34. Chen JY, Huang Y, Ortiz M. Fracture analysis of cellular materials: a strain gradient model. *J Mech Phys Solids*. 1998;26:789-828.
35. Lipperman F, Ryvkin M, Fuchs M. Fracture toughness of two dimensional cellular material with periodic microstructure. *Int J Fracture*. 2007;146(4):279-290.
36. Jelitto H, Schneider GA. A geometric model for the fracture toughness of porous materials. *Acta Mater*. 2018;151:443-453.
37. Jelitto H, Schneider GA. Fracture toughness of porous materials—Experimental methods and data. *Data Brief*. 2019;23:1-12, 103709.
38. Ryvkin M. Analytical solution for a mode III crack in a 3D beam lattice. *Intern J So Struc*. 2012;49(19-20):2839-2847.
39. Huang JS, Lin JY. Mixed-mode fracture of brittle cellular materials. *J Mater Sci*. 1996;31:2647-2652.
40. Srivastava V, Srivastava R. On the polymeric foams: modeling and properties. *J Mater Sci*. 2014;49(7):2681-2692.
41. Jang WY, Kyriakides S, Kraynik AM. On the compressive strength of open-cell metal foams with Kelvin and random cell structures. *Int J Solids Struct*. 2010;47(21):2872-2883.
42. Lu ZX, Liu Q, Huang JX. Analysis of defects on the compressive behaviors of open-cell metal foams through models using the FEM. *Mater Sci Eng A*. 2011;530:285-296.
43. Alkhader M, Vural M. An energy-based an isotropic yield criterion for cellular solids and validation by biaxial FE simulations. *J Mech Phys Solids*. 2009;57(5):871-890.
44. Daxner T. Finite element modelling of cellular materials. In: Altenbach H, Ochsner A, eds. *Cellular and Porous Materials in Structures and Processes*. Springer; 2010:47-106.
45. Ableidinger A. *Some Aspects of the Fracture Behavior of Metal Foams. Diploma Thesis*. Vienna: Vienna University of Technology; 2000.
46. Lee S-J, Wang J, Sankar BV. A micromechanical model for predicting the fracture toughness of functionally graded foams. *Intern J So Struc*. 2007;44(11-12):4053-4067.
47. Arakere NK, Knudsen EC, Wells D, McGill P, Swanson GR. Determination of mixed-mode stress intensity factors, fracture toughness, and crack turning angle for anisotropic foam material. *Intern J So Struc*. 2008;45(18-19):4936-4951.
48. Quintana-Alonso I, Mai SP, Fleck NA, Oakes DCH, Twigg MV. The fracture toughness of a cordierite square lattice. *Acta Mater*. 2010;58(1):201-207.
49. Wang J. *Fracture Toughness of Cellular Materials Using Finite Element Based Micromechanics*. Florida: A dissertation presented to the University of Florida; 2007.
50. Fleck NA, Qiu X. The damage tolerance of elastic-brittle, two dimensional isotropic lattices. *J Mech Phys Solids*. 2007;55(3):562-588.
51. Christodoulou I, Tan PJ. Crack initiation and fracture toughness of random Voronoi honeycombs. *Engin Frac Mech*. 2013;104:140-161.
52. Linul E, Marsavina L. Prediction of fracture toughness for open cell polyurethane foam by finite-element micromechanical analysis. *Iran Polym J*. 2011;20(9):735-746.
53. Murakami Y. *Stress Intensity Factors Handbook*. 1-2 Oxford: Pergamon Press; 1987.
54. Linul E, Serban DA, Marsavina L. Influence of cell topology on mode I fracture toughness of cellular structures. *Physical Mesome*. 2018;21(2):178-186.
55. Thiyagasundaram P, Wang J, Sankar BV, Arakere NK. Fracture toughness of foams with tetrakaidecahedral unit cells using finite element based micromechanics. *Engin Frac Mech*. 2011;78(6):1277-1288.
56. Settgast C, Abendroth M, Kuna M. Fracture mechanical analysis of open cell ceramic foams under multi-axial mechanical loading. *Arch Appl Mech*. 2016;86(1-2):335-349.

57. Rizov V, Mladensky A. Fracture behavior of HT-90 structural foam—A three-dimensional analysis. *Mate and De*. 2009; 30(3):617-621.
58. Landrock AH. *Handbook of Plastic Foams. Types, Properties, Manufacture and Applications*. Park Ridge: Noyes Publications; 1995.
59. Brown R. *Handbook of Polymer Testing: Physical Methods*. New York: Marcel Dekker Inc.; 1999.
60. Brown R. *Handbook of Polymer Testing*. Shawbury: Rapra Technology; 2002.
61. Ward IM, Sweeney J. *An Introduction to the Mechanical Properties of Solid Polymers*. 2nd ed. Chichester: John Wiley and Sons; 2004.
62. Park KB, Kim HT, Her NY, Lee JM. Variation of mechanical characteristics of polyurethane foam: effect of test method. *Dent Mater*. 2019;12(17):1-20, 2672.
63. ASTM. D5045-99: Standard Test Methods for Plane-Strain Fracture Toughness and Strain Energy Release Rate of Plastic Materials, 1999.
64. Poapongsakorn P, Carlsson LA. Fracture toughness of closed-cell PVC foam: effects of loading configuration and cell size. *Composite Struct*. 2013;102:1-8.
65. McIntyre A, Anderton GE. Fracture properties of a rigid PU foam over a range of densities. *Polymer*. 1979;20(2):247-253.
66. Viana GM, Carlsson LA. Mechanical properties and fracture characterisation of cross-linked PVC foams. *J Sanh Struc and Mate*. 2002;4:91-113.
67. Kabir ME, Saha MC, Jeelani S. Tensile and fracture behavior of polymer foams. *Mater Sci Eng A*. 2006;429(1-2):225-235.
68. Marsavina L, Linul E, Fracture toughness of polyurethane foams. Experiments versus micromechanical models, Proceedings of the 18th European Conference on Fracture, Dresden, Germany, 2010.
69. Burman M, Fatigue crack initiation and propagation in sandwich structures, Report No.98–29, Stockholm, 1998.
70. Andersons J, Cabulis U, Stiebra L, Kirpluks M, Sparniņš E. Modeling the mode I fracture toughness of anisotropic low-density rigid PUR and PIR foams. *Int J Fract*. 2017;205(1): 111-118.
71. Jin H, Lu W-Y, Scheffel S, Hinnerichs TD, Neilsen MK. Full-field characterization of mechanical behavior of polyurethane foams. *Intern J So Struc*. 2007;44(21):6930-6944.
72. Kidane A. On the failure and fracture of polymer foam containing discontinuities. *ISRN Materials Science*. 2013;408596. https://doi.org/10.1155/2013/408596
73. Apostol DA, Stuparu F, Constantinescu DM, Marsavina L, Linul E. Crack length influence on stress intensity factors for the asymmetric four-point bending testing of a polyurethane foam. *Materiale Plastice*. 2016;53(2):280-282.
74. Apostol DA, Constantinescu DM, Marsavina L, Linul E. Particularities of the asymmetric four-point bending testing of polyurethane foams. *UPB Sci Bull, Series D*. 2016;78(2):57-66.
75. Marsavina L, Constantinescu DM, Linul E, Apostol DA, Voiconi T, Sadowski T. Refinements on fracture toughness of PUR foams. *Engin Frac Mech*. 2014;129:54-66.
76. Marsavina L, Constantinescu DM, Linul E, Voiconi T, Apostol DA. Shear and mode II fracture of PUR foams. *Engin Fai Analy*. 2015;58:465-476.
77. Aliha MRM, Linul E, Bahmani A, Marsavina L. Experimental and theoretical fracture toughness investigation of PUR foams under mixed mode I+III loading. *Polymer Testing*. 2018;67: 75-83.
78. Bureau MN, Kumar V. Fracture toughness of high density polycarbonate microcellular foams. *J Cellular Plas*. 2006;42(3): 229-240.
79. Saenz EE, A., Carlsson LA, Karlsson A. Characterization of fracture toughness (Gc) of PVC and PES foams. *J Mater Sci*. 2011;46(9):3207-3215.
80. Matteson RC, Carlsson LA, Aviles F, Loup DC. On crack extension in foamed cored sandwich fracture specimens. In: Thomsen OT et al., eds. *Sandwich Structures 7: Advancing with Sandwich Structures and Materials*. Springer; 2005: 121-130.
81. Shivakumar K, Chen H, Bhargava A. Effect of geometric constraint on fracture toughness of PVC foam core sandwich beams. In: Thomsen OT et al., eds. *Sandwich Structures 7: Advancing with Sandwich Structures and Materials*. Springer; 2005:131-142.
82. Saenz EE, Carlsson LA, Karlsson AM. In situ analysis of crack propagation in polymer foams. *J Mater Sci*. 2011;46:5487-5494.
83. Saenz EE, Carlsson LA, Karlsson AM. In situ analysis of fatigue crack propagation in polymer foams. *Engin Frac Mech*. 2013;101:23-32.
84. Huber AT, Gibson LJ. Anisotropy of foams. *J Mater Sci*. 1988; 23(8):3031-3040.
85. Ganpatye AS, Kinra VK. Fracture toughness of space shuttle external tank insulation foam. In: 47th AIAA/ASME/ASCE/-AHS/ASC Structures, Structural Dynamics, and Materials Conference, Newport, Rhode Island, 2006.
86. Arvidson JM, Sparks LL. Low temperature mechanical properties of a polyurethane foam. National Bureau of Standards, U.S. Department of Commerce, Colorado 80303, 1981.
87. Farshidi A, Berggreen C, Carlsson LA. Low temperature mixed-mode debond fracture and fatigue characterisation of foam core sandwich. *J Sandw Struct Mater*. 2018;22(4):1039-1054. https://doi.org/10.1177/1099636218779420
88. Demharter A. Polyurethane rigid foam, a proven thermal insulating material for applications between +130°C and −196°C. *Cryogenics*. 1998;38(1):113-117.
89. Yakushin VA, Zhmud NP, Stirna UK. Physicomechanical characteristics of spray-on rigid polyurethane foams at normal and low temperatures. *Mech Compos Mater*. 2002;38(3): 273-280.
90. Stirna U, Beverte I, Yakushin V, Cabulis U. Mechanical properties of rigid polyurethane foams at room and cryogenic temperatures. *J Cell Plast*. 2011;47(4):337-355.
91. Denay AG, Castagnet S, Roy A, Alise G, Thenard N. Compression behavior of glass-fiber-reinforced and pure polyurethane foams at negative temperatures down to cryogenic ones. *J Cell Plast*. 2013;49(3):209-222.
92. Yakushin V, Cabulis U, Sevastyanova I. Effect of filler type on the properties of rigid polyurethane foams at a cryogenic temperature. *Mech Compos Mater*. 2015;51(4):447-454.
93. Knudsen E, Anisotropic fracture analysis of the BX-265 foam insulation material under mixed-mode loading, PhD Thesis, University of Florida, 2006.

94. Yu YH, Choi I, Nam S, Lee DG. Cryogenic characteristics of chopped glass fiber reinforced polyurethane foam. *Compos Struct*. 2014;107:476-481.
95. Fu SY, Lauke B. Effect of fiber length and fiber orientation distributions on the tensile strength of short fiber reinforced polymers. *Compos Sci Technol*. 1996;56(10):1179-1190.
96. Linul E, Marşavina L, Vălean C, Bănică R. Static and dynamic mode I fracture toughness of rigid PUR foams under room and cryogenic temperatures. *Eng Fract Mech*. 2020;225:1-10, 106274.
97. Bažant ZP. *Scaling of Structural Strength*. London: Hermes-Penton; 2002.
98. Bažant ZP, Yong Z, Goangseup Z, Isaac MD. Size effect and asymptotic matching analysis of fracture of closed-cell polymeric foam. *I J Solis Struct*. 2003;40:7197-7217.
99. Bažant ZP. Size effect in blunt fracture: concrete, rock, metal. *J Engin Mecha ASCE*. 1984;110(4):518-535.
100. Linul E, Marsavina L, Sadowski T, Kneć M. Size effect on fracture toughness of rigid polyurethane foams. *Solid State Pheno*. 2012;188:205-210.
101. Touliatou D, Wheel MA. K-dominance and size effect in mode I fracture of brittle materials with low to medium porosity. *Engin Frac Mech*. 2018;201:269-281.
102. Erdogan F, Sih GC. On the crack extension in plates under plane loading and transverse shear. *J Basic Engn*. 1963;85(4): 519-525.
103. Sih GC. Strain-energy-density factor applied to mixed mode crack problems. *I J Fract*. 1974;10(3):305-321.
104. Hussain MA, Pu SL, Underwood J, Strain energy release rate for a crack under combined mode I and mode II. In: Paris PC, Irwin GR, Editors, Fracture analysis, ASTM STP560, Philadelphia, 1974, 2–28.
105. Richard HA. *Bruchvorhersagen bei ueberlagerter Normal- und Schubbeanspruchung von Rissen*. Dusseldorf: VDI-Verlag; 1985.
106. Richard HA, Fulland M, Sander M. Theoretical crack path prediction. *Fatigue Fract Eng Mater Struct*. 2005;28(1-2):3-12.
107. Hallstrom S, Grenestedt JL. Mixed mode fracture of cracks and wedge shaped notches in expanded PVC foam. *I J Fract*. 1997;88(4):343-358.
108. Noury PM, Shenoi RA, Sinclair I. On mixed-mode fracture of PVC foam. *I J Fract*. 1998;92(2):131-151.
109. Linul E, Voiconi T, Marsavina L. Determination of mixed mode fracture toughness of PUR foams. *Struct Integ and Life*. 2014;14(2):87-92.
110. Linul E, Marsavina L. Experimental determination of mixed-mode fracture toughness for rigid polyurethane foams. In: Pluvinage G, Milovic L, eds. *Fracture at all Scales. Lecture Notes in Mechanical Engineering*. Springer; 2016:221-237.
111. Apostol DA, Constantinescu DM, Marsavina L, Linul E. Mixed-mode testing for an asymmetric four-point bending configuration of polyurethane foams. *Appl Mech Mater*. 2015; 760:239-244.
112. Marsavina L, Linul E, Voiconi T, Constantinescu DM, Apostol DA. On the crack path under mixed mode loading on PUR foams. *Frattura Ed Integrita Strutturale*. 2015;34:444-453.
113. Marsavina L, Constantinescu DM, Linul E, Stuparu FA, Apostol DA. Experimental and numerical crack paths in PUR foams. *Engin Frac Mech*. 2016;167:68-83.
114. Apostol DA, Stuparu F, Constantinescu DM, Marsavina L, Linul E. Experimental and XFEM analysis of mode II propagating crack in a polyurethane foam. *Materiale Plastice*. 2016; 53(4):685-688.
115. Lim IL, Johnston IW, Choi SK, Boland JN. Fracture testing of a soft rock with semi-circular specimens under three-point bending. Part 2—mixed-mode. *Int J Rock Mech Min Sci & Geomech Abstr*. 1994;31(3):199-212.
116. Wu EM. Application of fracture mechanics to anisotropic plates. *ASME J Appl Mech*. 1967;34(4):967-974.
117. Aliha MRM, Mousavi SS, Bahmani A, Linul E, Marsavina L. Crack initiation angles and propagation paths in polyurethane foams under mixed modes I/II and I/III loading. *Theore and Appl Frac Mecha*. 2019;101:152-161.
118. Mills NJ, Kang P. The effect of water immersion on the mechanical properties of polystyrene bead foam used in soft Shell cycle helmets. *J Cellular Plas*. 1994;30(3):196-222.
119. Marsavina L, Sadowski T. Dynamic fracture toughness of polyurethane foam. *Polymer Testing*. 2008;27(8):941-944.
120. Marsavina L, Linul E, Voiconi T, Sadowski T. A comparison between dynamic and static fracture toughness of polyurethane foams. *Polymer Testing*. 2013;32(4):673-680.
121. Rajak DK, Pagar DD, Menezes PL, Linul E. Fiber-reinforced polymer composites: manufacturing, properties, and applications. *Polymers*. 2019;11(10):1667.
122. Serban DA, Weissenborn O, Geller S, Marsavina L, Gude M. Evaluation of the mechanical and morphological properties of long fibre reinforced polyurethane rigid foams. *Polymer Testing*. 2016;49:121-127.
123. Linul E, Vălean C, Linul PA. Compressive behavior of aluminum microfibers reinforced semi-rigid polyurethane foams. *Polymers*. 2018;10(12):1298.
124. Linul E, Linul PA, Valean C, Marsavina L, Silaghi-Perju D. Manufacturing and compressive mechanical behavior of reinforced polyurethane flexible (PUF) foams. *IOP Conf Series: Mate Sci and Engin*. 2018;416:012053.
125. Członka S, Bertino MF, Strzelec K. Rigid polyurethane foams reinforced with industrial potato protein. *Polymer Testing*. 2018;68:135-145.
126. Cotgreave T, Shortall JB. The fracture toughness of reinforced polyurethane foam. *J Mater Sci*. 1978;13(4):722-730.
127. Chen CP, Gibson LJ. Fracture toughness performance indices for microsandwich foams. *J Mater Sci Lett*. 1995;14(9):665-667.
128. Wouterson EM, Boey FYC, Hu X, Wong S-C. Effect of fiber reinforcement on the tensile, fracture and thermal properties of syntactic foam. *Polymer*. 2007;48(11):3183-3191.
129. Maharsia RR, Jerro HD. Enhancing tensile strength and toughness in syntactic foams through nanoclay reinforcement. *Mater Sci Eng A*. 2007;454–455:416-422.
130. Wouterson EM, Boey FYC, Hu X, Wong S-C. Specific properties and fracture toughness of syntactic foam: effect of foam microstructures. *Composites Sci and Tech*. 2005;65(11-12): 1840-1850.
131. Wouterson EM, Boey FYC, Wong S-C, Chen L, Hu X. Nano-toughening versus micro-toughening of polymer syntactic foams. *Composites Sci and Tech*. 2007;67(14):2924-2933.
132. Stewart JK, Mahfuz H, Carlsson LA. Enhancing mechanical and fracture properties of sandwich composites using nanoparticle reinforcement. *J Mater Sci*. 2010;45(13):3490-3496.

133. Gómez-Monterde J, Sánchez-Soto M, Maspoch L. Microcellular PP/GF composites: morphological, mechanical and fracture characterization. *Composites: Part A*. 2018;104:1-13.
134. Idowu A, Boesl B, Agarwal A. 3D graphene foam-reinforced polymer composites. *A Review, Carbon*. 2018;135:52-71.
135. Nieto A, Boesl B, Agarwal A. Multi-scale intrinsic deformation mechanisms of 3D graphene foam. *Carbon*. 2015;85:299-308.
136. Jia J, Sun X, Lin X, Shen X, Mai YW, Kim JK. Exceptional electrical conductivity and fracture resistance of 3D interconnected graphene foam/epoxy composites. *ACS Nano*. 2014;8(6):5774-5783.
137. Patrick JF, Sottos NR, White SR. Microvascular based self-healing polymeric foam. *Polymer*. 2012;53(19):4231-4240.
138. Arencón D, Antunes M, Martínez AB, Velasco JI. Study of the fracture behavior of flexible polypropylene foams using the essential work of fracture (EWF). *Polymer Testing*. 2012;31(2):217-225.

How to cite this article: Marşavina L, Linul E. Fracture toughness of rigid polymeric foams: A review. *Fatigue Fract Eng Mater Struct*. 2020;1–32. https://doi.org/10.1111/ffe.13327